This is a preprint, the final version is subject to change, of the American Mineralogist (MSA)
Cite as Authors (Year) Title. American Mineralogist, in press.
(DOI will not work until issue is live.) DOI: http://dx.doi.org/10.2138/am.2013.4510 7/10

Revision 1

K-Ar dating and $\delta^{18}O$-δD characterization of nanometric illite from Ordovician K-bentonites of the Appalachians: Illitization and the Acadian-Alleghenian tectonic activity

Norbert Clauer[1], Anthony E. Fallick[2], Dennis D. Eberl[3], Miroslav Honty[4], Warren D. Huff[5] and Amélie Aubert[1]

[1] Laboratoire d'Hydrologie et de Géochimie de Strasbourg (CNRS-UdS),
1 rue Blessig, 67084 Strasbourg, France
[2] Scottish Universities Environmental Research Centre,
East Kilbride, Glasgow G75 0QF, UK
[3] Emeritus, U.S. Geological Survey, 3215 Marine St.,
Suite E127, Boulder, CO 08303, USA
[4] SCK-CEN, Health, Environment and Safety Institute,
Boeretang 200, 2400 Mol, Belgium
[5] Department of Geology, University of Cincinnati,
Cincinnati, OH 45221-0013, USA

Corresponding author: Dr. Norbert Clauer, Laboratoire d'Hydrologie et de Géochimie de Strasbourg, 1 rue Blessig, 67084 Strasbourg, France –
e-mail: nclauer@unistra.fr

Keywords: nanometric "fundamental" particles, XRD mineralogy, K-Ar dating, $\delta^{18}O$ and δD geochemistry, Ordovician K-bentonites, US Midcontinent, Acadian/Alleghenian orogeny

Abstract

Nanometric (<0.02, 0.02-0.05, 0.05-0.1, 0.1-0.2 μm) illite fractions were separated from K-bentonite samples from northwestern Georgia, and studied by X-ray diffraction, oxygen and hydrogen isotope geochemistry, and K-Ar dated in order to more tightly constrain the tectono-thermal history of the Appalachian orogeny. Their XRD patterns are very similar for a given sample with respect to the peak shapes and positions. They are ordered illite-smectite mixed layers with only small variations in the relative proportions of illite and smectite interlayers. The illite crystal thickness distributions also are very homogeneous across the various size fractions of the same sample, but crystallite thickness varies from sample to sample. It can be concluded from the α-β^2 diagram that illitization occurred in all fractions by simultaneous nucleation and crystal growth, except for one sample. In that sample, a period of growth without nucleation was detected on top of the nucleation and growth episode.

The K-Ar ages organize into two isochrons, the first at 319.9 $\pm$ 2.0 Ma with an initial $^{40}Ar/^{36}Ar$ ratio of 271 $\pm$ 66 Ma, and the second at 284.9 $\pm$ 1.2 Ma with an initial $^{40}Ar/^{36}Ar$ ratio of 310 $\pm$ 44. One data point above the older isochron and three between the two isochrons suggest a detrital contamination for the former separate and a possible further generation of nanoparticles for the three others. The samples with the older crystallization age consist of illite and illite-rich mixed-layers, and those with the younger age contain smectite-rich mixed-layers without illite, or illite-enriched illite-smectite mixed-layers. The K-Ar ages fit the age trends published previously for similar K-bentonites with regional age patterns between 240 and 270 Ma in the southwestern region, between 270 and 300 Ma in the central zone and the southern Appalachians, and between 315 and 370 Ma in the northernmost.

Each of the two generations of illite crystals yields very consistent $\delta^{18}O$ (V-SMOW) values at 17 $\pm$ 1‰ for the older and at 21 $\pm$ 1‰ for the younger. If crystallization temperatures of

the nanometric illite were between 100 and 200 °C, as suggested by microthermometric determinations, the hydrothermal fluids had $\delta^{18}O$ values of 4 ± 1‰ in the Dalton district and of 8 ± 1‰ in the Lafayette, Trenton and Dirtseller districts at 100 °C, and of 11 ± 1‰ and 15 ± 1‰ in the same locations at 200 °C, probably because the water-rock isotope exchanges at elevated temperature occurred in rock-dominated systems. The $\delta^{18}O$ of the fluids remained unchanged during local crystal growth, but varied depending on the geographic location of the samples and timing of illitization. The δD (V-SMOW) values of the different size fractions do not provide consistent information; they range from -70 to -45‰ for most nanometric and micrometric fractions (V-SMOW), but with no apparent coherent pattern.

Nanometric illite-rich crystals from K-bentonite that underwent tectono-thermal alteration yield constant ages, constant clay mineralogy, constant crystallite size distributions for all of the nucleating and growing illite-type crystals of each sample, as well as constant $\delta^{18}O$ values implying constant fluid chemistry, all pointing to geologically sudden crystallization.

Introduction

The outcrop area of Ordovician K-bentonites from the US midcontinent extends between Oklahoma to the southwest, Ontario to the northeast and Tennessee to the south with additional outcrops further to the southeast in Georgia and Alabama (Kolata et al. 1996; Leslie et al. 2008). The area is conventionally divided into several intracratonic basins and arches, including the foreland basins of the Appalachian and Ouachita orogens, once filled with thick sequences of Pennsylvanian and Permian sediments derived from the Alleghenian Orogeny (Beaumont et al. 1987). The Ordovician K-bentonites belong to a platform sedimentary sequence, where they are hosted by limestones overlain by a thick shale sequence resting on thick sandstone beds of Cambrian and Ordovician age and deposited on the Precambrian basement (e.g. Grathoff et al. 2001). Illitization of smectite from these K-bentonites was examined by Elliott and Aronson (1993) who reported a tendency toward a more smectitic composition with increasing distance from the orogenic front, the overall illite-smectite composition being locally quite homogeneous, even in the westernmost parts of the area (Hay et al. 1988). Lower smectite-layer occurrences in the clay material (<15%S) were recorded in the folded zone of the orogeny in the Appalachian Basin (Elliott and Haynes 2002). No compositional change was reported between the foreland

basin that may have experienced up to 3 km of Upper Paleozoic cover and the inter-cratonic areas where such cover was minimal (Beaumont et al. 1987). Numerous occurrences of authigenic K-feldspar were also documented in the bentonite beds of the western part of the area (Hay et al. 1988), as well as in the carbonate beds underlying the bentonite units of the Appalachian Basin (Hearn et al. 1987). An intense development of K-feldspar along with filamentous illite has also been documented below the bentonite beds over the whole cratonic area, in the St. Peter and Mt. Simon thick sandstone beds and in the regolith at the contact with the crystalline basement (Woodard 1972; Marshall et al. 1986; Harper et al. 1995; Duffin et al. 1989, Ziegler and Longstaffe 2000a; Chen et al. 2001; Liu et al. 2003).

The K-bentonite units containing well-crystallized illite-rich clay material are, therefore, interesting units to be isotopically dated for complementary reconstruction of the tectono-thermal activity of this midcontinental area. Available K-Ar data on illite-smectite from K-bentonites outline a clear regional pattern with younger ages between 240 and 270 Ma in the southwestern zone, intermediate ages between 270 and 300 Ma in the central zone and in the southern Appalachians, and older ages from 315 to 370 Ma towards the north (Elliott and Aronson 1987; 1993; Hay et al. 1988). Similar ages were recorded also for filamentous illite in the underlying sandstones (321-366 Ma; Girard and Barnes 1995; Ziegler and Longstaffe 2000b) and in the regolith (294-342 Ma; Ziegler and Longstaffe 2000a) to the north. This geographic distribution of K-Ar data parallels the tectonic events in the neighboring orogenic belt characterized by the late Devonian Acadian phase to the north and the Carboniferous-Permian Alleghenian phase in the more central and southern parts of the area.

The K-feldspar described in the Cambrian carbonate rocks and the illite-smectite of the Ordovician K-bentonites are contemporaneous in the southern Appalachian Basin, where fluid inclusions in the feldspar grains indicate a temperature range of 100-200 ^{o}C and a salinity of 18-21% NaCl equivalent for the interacting brines (Hearn et al. 1987; Elliott and Hayes 2002). Paleotemperatures well above 100 ^{o}C were also reported, both in the southern Appalachian Basin and the nearby foreland area (7-27% smectite layers in the illite-smectite mixed layer), on the basis of reset apatite fission tracks and partially reset zircon fission tracks (Roden et al. 1993). Long-distance migration of hot saline fluids has been invoked to explain these observations (Hearn et al. 1987; Elliott and Hayes 2002).

In the western midcontinent, the K-feldspars of the bentonite beds give clearly older K-Ar ages than the illite-smectite mixed layers (375-400 Ma; Hay et al. 1988). Similar or even older ages were obtained for K-feldspars from underlying rocks (Woodard 1972; Marshall et al. 1986; Duffin et al. 1989; Ziegler and Longstaffe 2000a; Chen et al. 2001; Liu et al. 2003). The petrographic evidence from sandstones indicates that K-feldspar and quartz crystallized at the same time, after the first generation illite-smectite, but before the second-generation illite-smectite (Fishman 1997). Fluid flow events of different nature are hypothesized to explain these observations.

Toulkeridis et al. (1998) dated biotite and clay separates of Ordovician K-bentonite units sampled in Alabama and Tennessee by the K-Ar, Sm-Nd and Rb-Sr methods. The biotite K-Ar ages at 459 $\pm$ 10 Ma were consistent with a Late-Ordovician deposition age for the bentonites. The clay fractions leached with dilute HCl provided a Sm-Nd isochron for the clay residues of 397 $\pm$ 44 Ma indicative of a crystallization during Acadian tectono-thermal activity at about 200°C, and a distinct younger Sm-Nd isochron of 285 $\pm$ 18 Ma for the acid leachates that represent distinct soluble mineral phases intimately associated with the clay particles. The Sm-Nd age of these non-silicate mineral phases is close to the K-Ar ages obtained previously on the clays in other areas of the eastern midcontinent, suggesting a thermally-induced recrystallization of the clay material but also of associated soluble minerals during the Alleghenian-Ouachita orogenic activity. The Rb-Sr system of the clay material was variably disturbed, except for the sample taken near the Allegheny Front for which an age of 179 $\pm$ 4 Ma suggests further tectono-thermal activity.

The age summary indicates that the tectonic and thermal history of the southern North American midcontinent is complex. The region experienced a thermal event of Acadian age recorded by the data of K-feldspars, and a further overprint by an Alleghenian thermal episode, which advanced the degree of the original illitization. It can therefore be considered that at least some of the available data generated from illite-smectite material represent mixing of illite contributions from the two events. Our attempt here to provide new information is based on the study of illite "fundamental" nanometric particles separated from illite-smectite mixed layers (labelled I/S hereafter) of K-bentonite units purposely collected close to the Alleghenian Front in Tennessee, together with one reference sample taken away from the front in Alabama, to: (1) date them with the K-Ar method to constrain tectonic/hydrothermal regional episodes independent of

the already available regional age cover; and (2) characterize the $\delta^{18}O$ and δD compositions of these nanometric crystals for new information on the oxygen and hydrogen isotope composition of the fluids that interacted with the nucleating and growing crystals and on the crystallization conditions of the illite crystals, in order to understand more about initial illitization in these volcanic materials.

The rationale for separating and analyzing nanometric I/S is that they normally consist of non-swelling coherent illite domains that are enriched in K and of smectite-type interlayers that are actually the shared expandable interfaces between adjacent illite crystals. Basically, the smaller the illite domains, the larger is the proportion of swelling interlayers that occur in the I/S structure. The illite crystals of such I/S were named "fundamental particles" by Nadeau et al. (1984) who were the first investigators to separate and examine these individual illite crystals. Their dispersion by infinite osmotic swelling allows "cleaning" of the swelling smectite-type interlayers that then become smectite-reacting surfaces of illite crystals, while the illite interlayers remain collapsed. As the term "fundamental" may be ambiguous to readers not fully familiar with these specific crystallographic studies, we have identified these crystals hereafter as "nanometric" relative to coarser separates, only referring to one-dimension of their size. The smectite-reacting surfaces of the illite crystals are termed smectite sites according to terminology used by Altaner and Ylagan (1997).

Geologic setting and sample description

Numerous K-bentonite beds have been described in the Ordovician carbonate rock-dominated sedimentary sequence of the eastern United States (Huff et al. 1986; Huff and Kolata 1990). They consist mainly of I/S resulting from alteration of felsic volcanic ash that induced progressive transformation of the initial smectite into illite. Isotopic support for basin-wide migration of hot saline fluids during this orogeny (Elliott and Aronson 1987; 1993) was also documented by $^{40}Ar/^{39}Ar$ ages between 278 and 322 Ma for authigenic K-feldspar crystals from Cambrian limestones throughout the central Appalachian basin (Hearn and Sutter 1985; Hearn et al. 1987). Remagnetization ages of ca 255 and 275 Ma were also reported across the central Appalachians related to folding and thrusting (Stamatakos et al. 1996). These results provided

new insights into the debate about movement of hot saline fluids through sedimentary basins (Dozy 1970; Garven and Freeze 1984; Bethke 1986; Oliver 1986; Bethke and Marshak 1990), knowledge of which is essential to elucidate how the K-bentonites evolved after deposition. The fact that the isotopic ages varied by up to 30-40 million years made it difficult to postulate a single continuous illitization process over this extended period of time. The present study was designed to refine and investigate in detail this age span, and also to identify specific regional events that have occurred during the entire Alleghenian-Acadian orogeny by analyzing smaller illite-rich size fractions than have been previously studied. The Middle-Upper Ordovician succession in the Allegheny Front is divided into a dominantly carbonate western facies and a largely siliciclastic eastern facies separated by the Helena thrust fault. Stratigraphic and sedimentologic descriptions are available in Drahovzal and Neathery (1971), Drahovzal and Neathery (1985), Raymond et al. (1988) and Szabo et al. (1988).

Nine samples were collected in northwestern Georgia at the boundary with Tennessee to the North and Alabama to the West (Fig. 1). They were taken close to the Allegheny Front, in an area delimited by the cities of Dalton, Lafayette and Trenton. Samples 1A and 1B are from Hamilton Mountain near Dalton, appearing in strata broken by small faults that belong to the 83-m thick Greensport Formation, which is composed of a lower unit of reddish gray, shaly, micritic limestone, a middle unit of red shale, and an upper unit of interbedded red shale and sandstone (Carter and Chowns 1989). The two samples represent respectively the base and the top of a 53 cm thick K-bentonite unit probably corresponding to the T3 Deicke bentonite of the Tennessee section. The 1A lower bed contains some thin interlayered red-shale beds, which could have resulted from some reworking during and immediately after deposition. The three samples 2A, 2B and 2C also coming from near Dalton represent the base, middle and top of a 60-cm thick K-bentonite bed probably corresponding to the T4 Millbrig K-bentonite of the Tennessee section. Sample 3A was taken about 8 miles NW of Lafayette, Georgia, near Davis Crossroads in the 15-30 m thick Carters Limestone, which is part of the Middle Ordovician Stones River Group in eastern Tennessee, and consists of fine-grained, yellowish-brown limestone, slightly cherty with several thin bentonite beds. Sample 3B is located S of Trenton in a 1 m thick unit interbedded with carbonate with some silicification. Sample 4A is the only one collected outside of Georgia; it comes from the Dirtseller Mountain quarry in Alabama and belongs to the Millbrig K-bentonite. Sample 4B belongs also to the Millbrig K-bentonite, but near Dalton, Georgia. A more

detailed stratigraphic positioning, especially for the Deicke and Millbrig samples, can be found in Kolata et al. (1996).

Analytical procedure

Whole-rock samples were crushed, sieved to 0.16 mm, and dropped into deionized water to be disaggregated using an ultrasonic bath. The <2 μm size fraction of each slurry was separated by sedimentation after treatment with sodium acetate, hydrogen peroxide and sodium dithionite according to Jackson's (1975) procedure. Recovered by high-speed ultracentrifugation, the <0.2 μm size fraction was further divided into four nanometric sub-fractions (<0.02, 0.02-0.05, 0.05-0.1 and 0.1-0.2 μm) by continuous-flow high-speed ultracentrifugation after infinite swelling, following Środoń et al. (1992). A combined chemical treatment and infinite swelling are applied to micrometric I/S to separate the non-swelling coherent illite domains with K-rich interlayers from smectite domains with K-depleted interlayers. The consequence is that the smectite-rich domains in the nanometric size fractions identified as such by XRD are most probably the shared expandable (swelling) interfaces between adjacent illite crystals. The excess soluble salts were removed by centrifugation and dialysis. X-ray diffraction (XRD) patterns were made on oriented air-dried (AD) and ethylene-glycolated (EG) specimens using a Siemens D500 XRD system with a graphite monochromator, CuKα radiation, a range of 2-32° 2θ, a step size of 0.02° 2θ and 5 seconds per step count time. The expandability (called $\%S_{XRD}$) was determined using a modified version of the delta two-theta method of Moore and Reynolds (1997) on the glycolated specimens:

$$\%S_{XRD} = 466.4 - 96.6\Delta + 5.0\Delta^2$$

where Δ represents the difference in two theta between the I/S peak at about 17° and the two-theta value for the peak at about 9°. This equation was derived from NEWMOD calculations.

The mean thickness and thickness distribution of the nanometric illite crystals were determined for the separated fine and ultrafine fractions by XRD after PVP-10 intercalation into the expandable interlayers to remove the cations held in the smectite-type interlayers and therefore improve subsequent X-ray diffraction analysis and measurement of crystallite size distributions, following Eberl et al. (1998a). Fundamental illite crystal thickness distribution (CTD) was determined from first-order reflections using the Bertaut-Warren-Averbach (BWA)

method (Drits et al. 1998) and the MudMaster program (Eberl et al. 1996). This method gives accurate measurements of mean thicknesses only for I/S particles that consist of less than 50% smectite layers, because the method is not able to detect smectite monolayers that potentially occur in more highly smectitic clays. Crystal-growth mechanisms that reproduce the measured CTDs of the different size fractions were simulated using the GALOPER program (Eberl et al. 2001). The volume-weighted and area-weighted mean thicknesses were calculated according to the BWA theory, and the parameters α (= mean of the natural logarithms of the thicknesses) and β^2 (= variance of the natural logarithms of the thicknesses) parameters were calculated from CTDs. These α and β^2 parameters of the different size fractions were plotted in a diagram along with other previously obtained results to evaluate the crystal growth reaction paths according to Eberl et al.'s (1998b) theory, in the manner of Bove et al. (2002).

The K-Ar determinations were made using a procedure similar to that of Bonhomme et al. (1975). Potassium was measured by flame spectrophotometry with an accuracy of 1.0%. For Ar analyses, the samples were preheated under vacuum at 80°C for at least 12h to reduce the amount of atmospheric Ar adsorbed on the mineral surfaces during sample preparation, separation and handling. The results were controlled by repetitive analysis of the GL-O glauconite standard, which averaged 24.57 $\pm$ 0.11 x 10^{-6} cm^3/g STP (2σ) of radiogenic ^{40}Ar for 5 independent determinations made during the course of the study. The $^{40}Ar/^{36}Ar$ ratio of the atmospheric Ar was also measured periodically, averaging 298.5 $\pm$ 1.0 (2σ) during the same period for 4 independent determinations. The recommended values being 24.85 $\pm$ 0.24 $\times$ 10^{-6} cm^3/g for the amount of radiogenic ^{40}Ar in the glauconite standard (Odin et al. 1982), and 295.5 for the atmospheric $^{40}Ar/^{36}Ar$ ratio (Nier 1950), the measured values were considered to be internally consistent with small uncertainties and close enough to the theoretical values not to require discrimination corrections to the individual determinations. The gas volume of the blank of the extraction line and the mass spectrometer was also determined before each Ar extraction. Systematically in the 10^{-8} cm^3 range, which is far below the contents of the different size fractions, the ^{40}Ar blank content was disregarded in the age calculations. The usual decay constants were used for the age calculations (Steiger and Jäger 1977), and the overall error is evaluated to be routinely better than 2% (2σ).

For the hydrogen isotope analyses, the samples were first vacuum-degassed at 200ºC overnight to remove the interlayer and absorbed surface water and were then transferred to a

previously out-gassed Pt crucible. The crucible was placed inside a quartz extraction chamber, which was then attached to the vacuum line and evacuated. Dehydroxylation was accomplished by radiofrequency induction heating of the crucible at 1200ºC. The released water was converted to H_2 by reaction with Cr at 800ºC (Bigeleisen et al. 1952; Donnelly et al. 2000*)* in a multiple-pass system. The H_2 yield was measured manometrically and δD determined on a gas-source mass spectrometer calibrated via water and mineral standards. With this analytical technique, the NBS30 biotite standard gave a δD of -65‰ (V-SMOW) and an analytical precision of ±6‰ (2σ) (see Fallick et al., 1993); this value represents the long-term reproducibility achieved by multiple analysts for an in-house kaolinite standard. The oxygen isotope composition of the clay minerals was determined by laser fluorination (Macaulay et al. 2000) based on the Borthwick and Harmon (1982) BrF_5 modification to Clayton and Mayeda's (1963) method. The long-term precision was ±0.6‰ (2σ) for an in-house quartz standard analyzed by multiple analysts, and the NBS28 quartz standard yielded a $\delta^{18}O$ of 9.6‰ (V-SMOW). All clay isotope data are reported in per mil (‰) relative to the V-SMOW standard. As indicated in Table 2, two duplicates of $\delta^{18}O$ values report internal reproducibility of $\pm$0.6 to $\pm$0.9% among the determinations. The stable isotope data reported here were all determined by one analyst over a short time interval; we propose that it is why the inter-sample consistency (see next section: Results) appears better than the long-term, multi-analyst technique precision quoted for $\delta^{18}O$; there was insufficient sample material to allow δD replicate analyses.

Results

XRD data

For any given sample, the XRD patterns of the AD nanometric size fractions are very similar with respect to the peak shapes and positions. They indicate that the size fractions contain ordered I/S of R3 Reichweite, which represents another way to quantify ordering of the I/S from disorder R0 type to highly ordered R3 type, with smectite-layer contents ranging from 6% to 23% (Moore and Reynolds 1997). Generally, the smectite-layer content does not change significantly with size fraction for a given sample, and kaolinite was detected in minute amounts in a few size

fractions (Table 1). Examples of XRD patterns for air-dried and glycol-solvated sample 4A are given in Figure 2 (A and B). Swelling was removed by PVP intercalation, and the resulting XRD patterns for the 001 peaks, shown for sample 4A in Figure 3, were analyzed by MudMaster program to yield mean crystallite thicknesses (Table 1) and crystallite thickness distributions, examples of which are given for sample 4A in Figure 4. The particle thickness distribution patterns are systematically very homogeneous for the different size fractions of the studied samples (Fig. 4), which is consistent with, but does not imply, that the coarser size fractions comprise aggregates of smaller particles.

In order to check the accuracy of the MudMaster-determined crystallite thickness distributions, the XRD pattern for glycolated sample 4A was back-calculated from crystallite thickness frequencies using the StackMan program (Eberl et al. 2011). This calculation assumes that I/S forms by the random stacking of illite crystals having different thicknesses. Smectite layers at the interfaces between crystals are considered to result from water and glycol adsorbed on crystal surfaces. For this calculation, it was assumed that each of the stacks (MacEwan crystallites) contains two illite crystals and, therefore, one smectite interlayer per stack. The frequency distribution determined by MudMaster program for sample 4A is given in Figure 5, as is the StackMan pattern that was calculated from these frequencies. The correspondence between calculated and measured patterns is excellent in peak intensity and location, thereby indicating that the thickness frequency distributions that were determined are accurate. The α-β^2 diagram confirms that, except for sample 3B, illitization occurred in all size fractions by the mechanism of simultaneous nucleation and growth, probably along a closed-system pathway that is expected for compacted bentonite beds (Fig. 6). The fractions of sample 3B that plot off this curve represent a growth mechanism that initially underwent a period of simultaneous nucleation and growth, followed by growth only (Bove et al. 2002). These fractions yield also the youngest K-Ar ages and could have crystallized in a geochemical system characterized by a higher degree of fluid circulation, explaining the two successive growth mechanisms.

A plot of volume or area-weighted mean crystallite thickness relative to the K-Ar age suggests no relation that is mathematically convincing between mean particle thickness and age (Fig. 7). However, it might be argued that the three fractions that have older individual ages at about 320 Ma appear to be slightly thicker (at 6 nm). This increase in the particle thickness of the older fractions could result from slightly more intense illitization. Also noteworthy are the values

of the water yields obtained in measuring the stable isotope compositions (Table 2): the narrow range, mostly from 2.7 to 3.3 μmol/mg, also suggests a very homogeneous particle composition of the size fractions.

$\delta^{18}O$ data

Twenty-five nanometric size fractions were analyzed for $\delta^{18}O$, which ranges from 15.8 to 22.2‰ (V-SMOW). Determination of the δD also provided precise measurements (± 10%) of the H_2O^+ content of the fractions (Table 2). The yields are scattered for the different size fractions of the same sample, with water contents of the coarser fractions either lower (samples 1A and 3A) or higher (samples 2A and 2C) than those of the two intermediate grain sizes. These variations do not clearly correspond either to the amounts of smectite-type swelling layers in the I/S structures (Table 1) or to variations of their $\delta^{18}O$.

The other notable analytical observation is that the nanometric size fractions of each sample have internally very consistent $\delta^{18}O$; the 2σ analytical dispersion never exceeds ± 0.4‰ for each set of values (see comment above in the Analytical Procedure section about dispersion). The $\delta^{18}O$ values for the eighteen size fractions from the six samples of the Dalton district range very narrowly from 15.8 ± 0.4‰ for sample 2B to 17.9 ± 0.1‰ for sample 1A (Table 2), whereas those from samples collected at Lafayette, Trenton and Dirtseller Mountain have systematically higher and also narrowly spread $\delta^{18}O$ values from 20.5 ± 0.1 to 22.2 ± 0.3‰.

δD data

The same twenty-five size fractions were also analyzed for δD; the values ranging widely from -90 to -26‰ (V-SMOW), although the spread is reasonably narrow for most size fractions of individual samples, apart from 1A and 2A samples (from –26 to –70‰ and from –64 to –90‰, respectively). The δD of the three size fractions of samples 2B, 3B and 4B vary very narrowly, whereas two of the three δD are close and the third quite distinct for samples 3A, 4A and 2C. In summary, there is no clear pattern apparent in the δD values, except that the δD values are equivalently narrowly scattered as the $\delta^{18}O$ values in some cases.

K-Ar data

The K-Ar ages of the different nanometric size fractions of each sample are almost identical throughout the suite of results (Table 3), significantly below the usual individual analytical uncertainty. Only the coarsest analyzed size fraction of sample 1B is significantly older than all other fractions. Such a distinct age is very seldom in K-bentonite units, especially in their nanometric fundamental particles (e.g. Clauer et al. 1997; Środoń and Clauer 2001; Środoń et al. 2006). The discrepancy for sample 1B most probably reflects a bias introduced by the addition of some detrital material from the overlying or underlying sedimentary unit during or after deposition, which although rare can occur due to some syn- or post-depositional reworking. This explanation is supported here by the occurrence of thin interbeds of red shale in the K-bentonite unit.

The data range narrowly within 2 Ma for the size fractions of samples 4A and 3B, within 3 Ma for those of samples 3A, 2B, 2A and 1B, within 5 Ma for those of samples 1A and 2C after discarding the age of the coarsest fraction, and within 6 Ma for those of sample 4B. Also, the K-Ar ages are very similar for the nanometric fractions at the base and top of the same K-bentonite beds. For instance, the average values of the size fractions from samples 1A and 1B are within 1 Ma, and the base and intermediate layers of sample 2A and 2B are within 3 Ma, whereas the top sample 2C appears to have reacted longer (or later) by 10 to 14 Ma.

The entire set of K-Ar ages ranges from 279 $\pm$ 7 to 324 $\pm$ 8 Ma, which is similar to those available in the literature from the same area (Hearn and Sutter 1985; Hearn et al. 1987; Elliott and Aronson 1987; 1993; Hay et al. 1988). However, a detailed look at the results shows four tightly-grouped average ages at 279-281 Ma for samples 3A and 3B, 304-305 Ma for samples 2C and 4B, 310-312 Ma for the samples 2A and 2B, and 317-318 for the samples 1A and 1B. Only the sample collected away from the Allegheny Front provides a set of K-Ar ages that is in between the two young age averages at about 293 $\pm$ 2 Ma. Notwithstanding the fact that the number of studied samples is limited, it is interesting that each "step" in age has been recorded in all nanometric size fractions of two distinct samples having very similar mineral compositions and $\delta^{18}O$ values. This suggests that the distinct steps could have geological meaning especially since the age data do not overlap.

A plot of the $^{40}Ar/^{36}Ar$ versus $^{40}K/^{36}Ar$ yields two straight lines, and four data points lying off these lines: three between the two lines and one above the upper of the two lines (Fig. 8). The characteristics of the two lines respectively correspond to an age of 319.9 $\pm$ 2.0 Ma for the upper

line with an initial $^{40}Ar/^{36}Ar$ ratio of 271 $\pm$ 66, and 284.9 $\pm$ 1.2 Ma for the lower line with an initial $^{40}Ar/^{36}Ar$ of 310 $\pm$ 44. The isochron age of each line is within the uncertainty of the mean age of the samples that define the isochron, and the uncertainties of the intercept values of both isochrons clearly include the value of the atmospheric $^{40}Ar/^{36}Ar$ ratio; each of these facts supports the assumption that the ages are geologically meaningful.

Because of the volcanic origin of bentonite units some of the authigenic clay-type minerals, especially the I/S mixed-layers such as those studied here, contain small and variable amounts of NH_4, which substitutes for K^+ in the interlayer sites (e.g. Nadeau and Bain 1986). However, such substitution does not affect the K-Ar age of the separated I/S, which strictly and only depends on the K/radiogenic ^{40}Ar ratio of the separated mineral particles, as has been shown in a dedicated K-Ar dating study of NH_4-illite rich I/S (Clauer et al. 2010).

Discussion

Depending on the mechanism of illitization, one may expect different isotopic ages for nanometric illite crystals as they theoretically grow thicker and larger with time. The crystal growth theory of Eberl et al. (1998b) predicts that the growth rate is proportional to crystal size, indicating that the isotopic ages of the coarser fractions may be younger than those of the finer, because the coarser crystals add new material at a faster rate than the finer crystals. This assumption was confirmed by the first K-Ar ages of bentonite beds from the East-Slovak Basin but not in the nearby Zempleni Mountains where illite crystallized from hot hydrothermal fluids (Clauer et al. 1997). Illitization of nanometric clays sampled from drill-holes of the basin lasted for several millions of years, whereas the various size fractions of the hydrothermal Zempleni clays provided a single age within analytical uncertainty. The duration of illitization depends on the driving parameters, and one can imagine two end-member histories: (1) a slow process accompanied by progressive temperature increase during burial, and (2) a rapid process with an essentially instantaneous temperature increase during a hydrothermal overprint. Such varied processes were reported in several studies (e.g. Clauer et al. 1997; Środoń and Clauer 2001; Honty et al. 2004; Środoń et al. 2006; Clauer et al. 2013). Because we found homogeneous ages for the nanometric fractions of any given sample, as well as homogeneous mineral compositions, crystallite thickness distributions and reaction mechanisms, we are inclined to believe that the

illitization of our samples occurred under abnormal episodic thermal conditions that provided narrow (i.e. within analytical uncertainty) ages of the different nanometric particles, as opposed to ages ranging beyond analytical uncertainty when recording burial-induced diagenetic crystal growth (e.g. Clauer et al. 2013). Only in the case of sample 4B, the finest (<0.02 μm) fraction is slightly, at the analytical limit, younger than the two coarser (0.02-0.05 and 0.1-0.2 μm) fractions (Table 3), which suggests that two nucleation episodes occurred successively in this sample.

Geological meaning of the K-Ar ages

The individual K-Ar ages obtained for the different size fractions for each of our samples are slightly higher for the basal layers relative to the equivalent top-layer samples. This is the case for the samples 1A and 1B, and 2A, 2B and 2C collected from T3 and T4 bentonite units near Dalton, Georgia, but the age difference remains within analytical uncertainty. It looks as if, although induced by temperature increase and migration of hydrothermal fluids from nearby tectonic activity, illitization lasted slightly longer at the basal parts of the bentonite units.

There is no visible correlation between the K-Ar ages and the geographic dispersion of the samples: the younger ages were obtained on the northern Trenton, the central Lafayette and the southern Dirtseller sites. The K-Ar ages of illite-type nanometric particles from K-bentonite samples collected in Georgia and Alabama point to the occurrence of two hydrothermal overprints induced by nearby tectonic activity at 319 $\pm$ 2.0 and 284.9 $\pm$ 1.2 Ma. An additional pulse could have happened in between at 293 $\pm$ 2 Ma, but this needs to be confirmed. These K-Ar ages fit in the trends published previously on similar illite-smectite mixed layers from similar bentonite beds with regional age patterns between 240 and 270 Ma in the southwestern zone, between 270 and 300 Ma in the central zone and in the southern Appalachians, and from 315 to 370 Ma to the north (Elliott and Aronson 1987; 1993; Hay et al. 1988; Toulkeridis et al. 1998). The lower K-Ar age of the finest (<0.02 μm) fraction of sample 4B relative to the two coarser suggests a two-step crystallization, but the $\delta^{18}O$ values of this slightly younger fraction is not that of all the other younger nanometric fractions: <17.0 relative to >20.5‰. This difference in the $\delta^{18}O$ rather points rather to the analytical uncertainty on the K-Ar ages than to episodic nucleation and growth.

Restored into the regional structural evolution, both the previously published ages and those released here correlate well with the general understanding of the Late Paleozoic tectonic history of the southern Appalachians. The hinterland is partially composed of a complex mosaic of terranes that were amalgamated to the Laurentian margin during multiple phases of collision and related magmatism throughout Paleozoic time (Beaumont et al., 1987; Hatcher, 2002). The culminating orogenic event of the Appalachians is the Late Mississippian–Pennsylvanian Alleghanian episode that involved an oblique, transpressive, and rotational collision between parts of Gondwana and previously accreted peri-Gondwanan assemblages, causing the formation of the Pangean supercontinent (Hatcher et al., 1989). In the central and southern Appalachians, the Alleghenian orogeny involved: (1) accretion of the Archean Suwannee terrane to the southeast margin of Laurentia (Horton et al., 1989), (2) lateral translation of previously accreted terranes along dextral strike-slip faults (Hatcher, 2002), (3) a 300–325 Ma subduction-related magmatism and greenschist to amphibolite facies regional metamorphism of hinterland terranes (Hatcher et al., 1989; Hatcher, 2005), and (4) development of a foreland fold-thrust belt that propagated into sedimentary rocks from the allochthonous pre-Alleghenian metamorphic rocks in the southern and central Appalachians (Hatcher et al., 1989). The final stage of the Alleghenian scenario involved head-on collision of southeastern Laurentia with Gondwana (Horton et al., 1989). The major product of head-on collision is the Blue Ridge–Piedmont megathrust sheet that transported crust amalgamated during all previous Paleozoic events at least 350 km onto the North American platform. The collision was finished about 265 Ma, forming supercontinent Pangaea and completing the Paleozoic Wilson Cycle of opening and closing of oceans.

Significance of the $\delta^{18}O$ values

The $\delta^{18}O$ values of the nanometric-to-micrometric sub-fractions of the different samples are internally very consistent. Interestingly, the fluid temperature and $\delta^{18}O$ composition can therefore likely be considered to be constant throughout the different bentonite beds known for their very low porosity and permeability. This could mean that illitization occurred when the bentonites were still somehow porous, consisting of volcanic glass in contact with locally isotopically homogeneous fluids.

Previous studies of authigenic feldspar fluid-inclusion microthermometric determinations from the same geographic area indicate a temperature range of 100-200 ^{o}C and a salinity of 18-

21% NaCl equivalent for the interacting brines (Hearn et al. 1987; Elliott and Hayes 2002). Paleotemperatures well above 100 ^{o}C were also evidenced by completely reset apatite fission tracks and partially reset zircon fission tracks (Roden et al. 1993). Inserting the reference temperatures of 100 to 200 °C, which relate to the tectonic activity described in this region (Smith 2006), together with the $\delta^{18}O$ of 16 to 18‰ and of 20 to 22‰ for the two generations of illite, into the illite-water equilibrium oxygen isotope fractionation equation (Sheppard and Gilg 1996):

$$1000\ln a^{18}_{illite\text{-}water} = 2.39\ 10^{6}T^{-2} - 4.19$$

gives $\delta^{18}O$ of about 4 $\pm$ 1‰ for the fluids at 100 °C in the Dalton district and of about 8 $\pm$ 1‰ in the Lafayette, Trenton and Distseller districts. The $\delta^{18}O$ values of the same fluids would be 11 $\pm$ 1‰ and 15 $\pm$ 1‰ in the two districts, respectively, at a temperature of 200 °C. Assuming that illite precipitated at isotopic equilibrium, the $\delta^{18}O$ of the parental fluids did not change during local crystal growth, as the $\delta^{18}O$ values are systematically very homogeneous (range of 0.1 to 0.9‰ for the extreme $\delta^{18}O$ values for each set of analyzed size fractions), but it expectedly changed with the geographic location of the samples and the timing of illitization. Further useful discussion would require better constrained temperature estimates, which might allow a deeper insight as to how the chemical and isotopic characteristics of the fluids parental to the illite varied in time and space. What is clear, however, is that the high $\delta^{18}O$ values calculated from the measured illite $\delta^{18}O$ compositions and the assumed temperatures strongly suggest isotope exchange at elevated temperature in a rock-dominated system.

The significantly higher $\delta^{18}O$ values of the illite crystals from the Lafayette, Trenton and Dirtseller districts that precipitated later at about 285 Ma, suggest that the crystallization temperature was lower (Fig. 9A and B). An alternative suggestion is that the water $\delta^{18}O$ was higher during the more recent tectonic activity due to more pervasive water-rock interaction in a rock-dominated system (e.g. Aagard and Egeberg 1998), unless both, a lower crystallization temperature and a higher fluid $\delta^{18}O$ were combined.

Information from δD values

As discussed previously, the δD values of the different size fractions do not give a consistent pattern, as was also found for illite-enriched nanometric particles from bentonite units of the East Slovak Basin (Clauer et al., 2013). Therefore, the δD results do not support a systematic occurrence of agglomerated nanometric particles in the different size fractions, because there is no consistent evidence of δD being the same from fine to coarse particles within a given sample, and additionally $\delta^{18}O$ does not change as significantly as δD (Fig. 9). Other factors having a significant impact on the illite δD values could have varied, depending for instance on the immediate environment of the nucleating and growing crystals, and also on potential exchange with ground waters since crystallization (Longstaffe and Ayalon 1990).

Variable initial $\delta^{18}O$-δD composition of the hydrothermal fluids resulting from a long-lived illitization process is not a viable model here, because illitization is considered to be almost instantaneous in the present case. The $\delta^{18}O$ of the fluids appears then to depend on geographic location and crystallization timing with probable varied thermal gradients, changing water/rock interactions, or on other processes not yet identified. Beyond these aspects, differences in the nucleation and growth processes may induce changes in δD, and therefore could result in changing $^{18}O/^{16}O$ and D/H of the hydroxyl groups because of interaction with changing fluids during particle growth. Whilst the capacity for isotope resetting during post-precipitation processes is still debated, it is clear that D/H is more susceptible to such changes than $^{18}O/^{16}O$ (e.g. Bird and Chivas 1988; Longstaffe and Ayalon 1990, and references therein).

The extremely constant $\delta^{18}O$ values of the different nanometric illite fractions represents a strong argument against changing fluids during the nucleation and growth processes, and also against post-precipitation changes of the hydroxyls, as about half of the illite oxygen is present as hydroxyls in the mineral structure. Bechtel and Hoernes (1990) estimated that isotope fractionation between framework and hydroxyl oxygen in illite is about 15‰ at 200 °C, and even higher at lower temperature, so constant mineral $\delta^{18}O$ implies little post-precipitation exchange of hydroxyl oxygen. Clearly, except if proton exchange allowing H isotopic composition of hydroxyls to change without affecting the O isotopic composition, such intra-mineral considerations do not influence D/H and so cannot explain the δD scatter obtained here. Until such a proton-exchange hypothesis is tested, we decided to report, even though without a satisfactory explanation, to contribute to the still limited analytical database. Initial smectite layers may also preserve interlayer water of an isotopic composition acquired from the

551 environment prior to illitization. However, the specific sample preparation with PVP polymer and
552 the infinite osmotic dispersion cleans the smectite interlayers of the crystals by removing the
553 cations and could, perhaps, alter the structural hydroxyl D/H. This would imply hydrogen isotope
554 exchange at low temperature over a very short hourly timescale, which of course needs also to be
555 checked specifically.
556

557 ## Conclusions

558

559 K-bentonite samples collected in northwestern Georgia at the boundary with Tennessee to
560 the north and Alabama to the west consist of illite/smectite mixed-layers that were separated into
561 varied nanometric (<0.02, 0.02-0.05, 0.05-0.1, 0.1-0.2 μm) size fractions. Most are R3 ordered
562 and very similar for a given sample with respect to the XRD peak shapes and positions. Based on
563 the α-β^2 diagram, illitization occurred by simultaneous nucleation and crystal growth along a
564 rather closed-system pathway, except in one sample where only growth was detected after initial
565 nucleation, suggesting a different more open crystallization environment. Two K-Ar isochrons
566 were obtained at 319.9 $\pm$ 2.0 Ma with an initial $^{40}Ar/^{36}Ar$ ratio of 271 $\pm$ 66, and at 284.9 $\pm$ 1.2 Ma
567 with an initial $^{40}Ar/^{36}Ar$ ratio of 310 $\pm$ 44. A possible additional generation of nanoparticles could
568 have crystallized at about 293 $\pm$ 2 Ma, which might represent a continuous but slow crystal
569 growth after the older thermal episode, in a region without further pronounced thermal activity in
570 an environment favorable for illitization. This hypothesis needs, of course, to be confirmed. The
571 obtained K-Ar ages fit the age trends published previously for similar K-bentonites with regional
572 age patterns between 240 and 270 Ma to the southwest, between 270 and 300 Ma in the central
573 and the southern Appalachians, and between 315 and 370 Ma to the north.

574 The determined K-Ar ages correlate well with the general understanding of the Late
575 Paleozoic tectonic history of the southern Appalachians. The culminating orogenic event is the
576 Late Mississippian–Pennsylvanian episode that involved an oblique, transpressive, and rotational
577 collision between parts of Gondwana and previously accreted peri-Gondwanan assemblages. In
578 the central and southern Appalachians, the Alleghenian orogeny involved also the development of
579 a foreland fold-thrust belt that propagated into sedimentary rocks from the allochthonous pre-
580 Alleghenian metamorphic rocks in the southern and central Appalachians that ended about 265
581 Ma ago.

582 The two generations of illite crystals yield extremely constant $\delta^{18}O$ values at 17 $\pm$ 1‰ for
583 the older and at 21 $\pm$ 1‰ for the younger. If crystallization temperatures of the nanometric illite
584 were between 100 and 200 °C, as suggested by microthermometric measurements, the interacting
585 fluids were of hydrothermal origin with $\delta^{18}O$ values of 4 $\pm$ 1‰ in the Dalton district and of 8 $\pm$
586 1‰ in the Lafayette, Trenton and Dirtseller districts at an implied temperature of 100 °C, and of
587 11 $\pm$ 1‰ and 15 $\pm$ 1‰ in respectively the same locations at an implied temperature of 200 °C. If
588 illite precipitated at isotopic equilibrium, the $\delta^{18}O$ of the fluids remained unchanged during local
589 crystal growth, but varied depending on the geographic location of the samples and timing of
590 illitization. The widely scattered δD values, from -70 to -45‰ (V-SMOW) for most size
591 fractions.
592 The combined mineralogical XRD study applied to nanometric illite-type crystals to
593 assess their crystal thickness distribution provides further insights into illitization, together $\delta^{18}O$
594 and δD isotopic determinations, such as controlled constant ages, constant clay mineralogy,
595 constant crystallite size distributions for all of the nucleating and growing illite-type crystals of
596 each sample, constant $\delta^{18}O$ values implying constant fluids. All these parameters point to
597 geologically sudden crystallization episodes that support episodic tectono-thermal activity.
598 Complementary K-Ar dating shows that the samples from different locations reacted at different
599 times, with only one sample deviating from concomitant nucleation and growth process.
600 However, the restricted number of samples makes it difficult to enlarge the picture to a regional
601 scale including the search for migration of heat sources and associated fluid flows, as well as
602 timing of their occurrence(s).
603

604 ## Acknowledgements

605

606 We are deeply indebted to the two reviewers F.J. Longstaffe and D. Awwiller for their
607 very thoughtful and constructive comments that helped improving and focusing the previous draft
608 of this note. We are also thankful to the editorial board, especially to Chief Editor H. Xu for very
609 efficient handling of the review round. We would like also to extend sincere thanks to Sam
610 Chaudhuri for having organized the sampling together with Tim Chowns, S. Holland and P.
611 Schroeder, to Jan Środoń for separation of the nanometric size fractions at the Geological

Institute PAN of Krakow, Poland, and to Robert Wendling, Raymond Wendling, Daniel Tisserant and Raymond Winkler of the Centre de Géochimie de la Surface (CNRS/ULP) for technical assistance during the study. SUERC was supported by NERC and a consortium of Scottish Universities.

References

Altaner, S.P. and Ylagan, R.F. (1997) Comparison of structural models of mixed-layer illite/smectite and reaction mechanisms of smectite illitization. *Clays and Clay Minerals*, 45, 517-533.

Beaumont, C., Quinland, G.M. and Hamilton, J. (1987) The Alleghanian orogeny and its relationship to the evolution of the Eastern Interior, North America. In: Beaumont C and Tankard A.J. (eds.), Sedimentary Basins and Basin-Forming Mechanisms. *Canadian Society of Petroleum Geologists Memoir*, 12, 425-445.

Bechtel, A. and Hoernes, S. (1990) Oxygen isotope fractionation between oxygen of different sites in illite minerals: A potential single-mineral thermometer. *Contribution to Mineralogy and Petrology*, 104, 463-470.

Bethke, C.M. (1986) Hydrologic constraints on the genesis of the Upper Mississippi Valley mineral district from Illinois basin brines. *Economic Geology*, 81, 233-249.

Bethke, C.M and Marshak, S. (1990) Brine migrations across North America – the plate tectonics of groundwater. *Annual Review of Earth and Planetary Sciences*, 18, 287-315.

Bigeleisen, J., Perlman, M.L. and Prosser, H.C. (1952) Conversion of hydrogenic materials to hydrogen for isotopic analysis. *Analytical Chemistry*, 24, 356-1357.

Bird, M.I. and Chivas, A.R. (1988) Stable-isotope evidence for low temperature kaolinitic weathering and post-formational hydrogen-isotope exchange in Permian kaolinites. *Chemical Geology (Isotope Geosciences)*, 72, 249-265.

Bonhomme, M., Thuizat, R., Pinault, Y., Clauer, N., Wendling, A. and Winkler, R. (1975) Méthode de datation potassium–argon appareillage et technique. In: Notes Techniques de l'Institut de Géologie, Université Louis Pasteur, Strasbourg, 3, 53 p.

Borthwick, J. and Harmon, R.S. (1982) A note regarding ClF_3 as an alternative to BrF_5 for oxygen isotope analysis. *Geochimica et Cosmochimica Acta*, 46, 1665-1668.

643 Bove, D.J., Eberl, D.D., McCarty, D.K. and Meeker, G.P. (2002) Characterization of modeling of
644 illite crystal particles and growth mechanisms in a zoned hydrothermal deposit, Lake City,
645 Colorado. *American Mineralogist*, 87, 1546-1556.
646 Brooks, C., Hart, S.R. and Wendt, I. (1972) Realistic use of two-error regression treatments as
647 applied to rubidium–strontium data. *Reviews of Geophysics and Space Physics*, 10, 551–577.
648 Carter, B.D. and Chowns, T.M. (1989) Stratigraphic and environmental relationships of Middle
649 and Upper Ordovician rocks in Northwest Georgia and Northeast Alabama. In Keith B.D.
650 (ed.), The Trenton Group (Upper Ordovician Series) of Eastern North America, Deposition,
651 Diagenesis, Tetroleum. *American Association of Petroleum Geologists Studies in Geology*, 29,
652 17-26.
653 Chen, Z., Riciputi, L.R., Mora, C.I. and Fishman, N.S. (2001) Regional fluid migration in the
654 Illinois basin: evidence from in situ oxygen isotope analysis of authigenic K-feldspar and
655 quartz from the Mount Simon Sandstone. *Geology*, 29, 1067-1070.
656 Clauer, N., Środoń, J., Francu, J. and Šucha, V. (1997) K-Ar dating of illite fundamental particles
657 separated from illite-smectite. *Clay Minerals*, 32, 181-196.
658 Clauer, N., Liewig, N. and Bobos, I. (2010) K-Ar, $\delta^{18}O$ and REE constraints on the genesis of
659 ammonium illite from the Harghita Bai hydrothermal system, Romania. *Clay Minerals*, 45,
660 393-411.
661 Clauer, N., Honty, M., Fallick, A.E., and Šucha, V. (2013) Regional illitization in bentonite beds
662 from East Slovak Basin based on isotopic characteristics (K-Ar, $\delta^{18}O$ and δD) of illite-type
663 nanoparticles. *Clay Minerals*, accepted.
664 Clayton, R.N. and Mayeda, T.K. (1963) The use of bromine pentafluoride in the extraction of
665 oxygen from oxides and silicates for isotopic analysis. *Geochimica et Cosmochimica Acta*, 27,
666 43-52.
667 Donnelly, T., Waldron, S., Tait, A., Dougans, J. and Bearhop, S. (2000) Hydrogen isotope
668 analysis of natural abundance and deuterium-enriched waters by reduction over chromium on-
669 line to a dynamic dual inlet isotope-ratio mass spectrometer. *Rapid Communications In Mass*
670 *Spectrometry*, 15, 1297-1303.
671 Dozy, J.J. (1970) A geological model for the genesis of the lead-zinc ores of the Mississippi
672 Valley, USA. *Transactions International Mining and Metallogeny, Section B*, 79, 163-170.
673 Drahovzal, J.A., and Neathery, T.L. (1971) The middle and upper Ordovician stratigraphy of the

Alabama Appalachians, In: The middle and upper Ordovician stratigraphy of the Alabama Appalachians, Drahovzal, J.A. and Neathery T.L. (eds.), *Alabama Geological Society Guidebook for the Ninth Annual Fieldtrip*, 1-62.

Drahovzal, J.A., and Neathery, T.L. (1985) Lithostratigraphy of Upper Ordovician strata in Alabama. *Alabama Geological Survey Circular*, 124, 55p.

Drits, V.A., Eberl, D.D. and Środoń, J. (1998) XRD measurement of mean thickness, thickness ditribution and strain for illite and illite/smectite crystallites by the Bertaut-Warren-Averbach technique. *Clays and Clay Minerals*, 46, 461 - 475.

Dudek, T. and Środoń, J. (1996) Identification of illite/smectite by X-ray powder diffraction taking into account the lognormal distribution of crystal thickness. *Geologica Carpathica*, 5, 21-32.

Duffin, M.E., Lee, M., de V. Klein, G. and Hay, R.L. (1989) Potassic diagenesis of Cambrian sandstones and Precambrian granitic basement in UPH-3 deep hole, Upper Mississippi Valley, USA. *Journal of Sedimentary Petrology*, 59, 848-861.

Eberl, D.D. and Środoń, J. (1988) Ostwald ripening and interparticle-diffraction effects from illite crystals. *American Mineralogist*, 73, 1335-1345.

Eberl, D.D., Drits, V., Środoń, J. and Nüesch, R. (1996) MudMaster: a program for calculating crystallite size distribution and strain from the shapes of X-ray diffraction peaks. *U. S. Geological Survey, Open-File Report*, 96-171.

Eberl, D.D., Nüesch, R., Šucha, V. and Tsipursky, S. (1998a) Measurement of fundamental illite particle thickness by X-ray diffraction using PVP-10 intercalation. *Clays and Clay Minerals*, 46, 89-97.

Eberl, D.D., Drits, V.A. and Środoń, J. (1998b) Deducing growth mechanisms for minerals from the shapes of crystal size distributions. *American Journal of Sciences*, 298, 499-533.

Eberl, D.D., Drits, V.A. and Środoń, J. (2001) User's guide to GALOPER – a program for simulating the shapes of crystal size distributions – and associated programs. *U.S. Geological Survey, Open-File Report,* OF00-505, 44p.

Eberl, D.D., Blum, A.E., and Serravezza, M. (2011) Anatomy of a metabentonite: nucleation and growth of illite crystals and their coalescence into mixed-layer illite/smectite. *American Mineralogist*, 96, 586-595.

704 Elliott, W.C. and Aronson, J.L. (1987) Alleghanian episode of K-bentonite illitization in the
705 southern Appalachian Basin. *Geology*, 15, 735-739.
706 Elliott, W.C. and Aronson, J.L. (1993) The timing and extent of illite formation in Ordovician K-
707 bentonites at the Cincinnati Arch, the Nashville Dome and north-eastern Illinois basin. *Basin*
708 *Research*, 5, 125-135.
709 Elliott, W.C. and Haynes, J.T. (2002) The chemical character of fluids forming diagenetic illite in
710 the Southern Appalachian Basin. *American Mineralogist*, 87, 1519-1527.
711 Fallick, A.E., Macaulay, C.I. and Haszeldine, R.S. (1993) Implications of linearly correlated
712 oxygen and hydrogen isotopic compositions for kaolinite and illite in the Magnus Sandstone,
713 North Sea. *Clays and Clay Minerals*, 41, 184-190.
714 Fishman, N.S. (1997) Basin-wide fluid movement in a Cambrian paleoaquifer: evidence from the
715 Mt. Simon Sandstone, Illinois and Indiana. In: Basin-Wide Diagenetic Patterns: Integrated
716 Petrologic, Geochemical, and Hydrologic Considerations, *Society of Economic Paleontologists*
717 *and Mineralogists, Special Publication*, 57, 221-234.
718 Garven, G. and Freeze, R.A. (1984) Theoretical analysis of the role of groundwater flow in the
719 genesis of stratabound ore deposits. 1. Mathematical and numerical model and 2. Quantitative
720 results. *American Journal of Science*, 284, 1085-1174.
721 Girard, J.P. and Barnes, D.A. (1995) Illitization and paleothermal regimes in the Middle
722 Ordovician St. Peter Sandstone, central Michigan basin: K-Ar, oxygen isotope, and fluid
723 inclusion data. *American Association of Petroleum Geologists Bulletin*, 79, 49-69.
724 Grathoff, G.H., Moore, M.M., Hay, R.L. and Wemmer, K. (2001) Origin of illite in the lower
725 Paleozoic of the Illinois basin: evidence for brine migrations. *Geological Society of America*
726 *Bulletin*, 113, 1092-1104.
727 Harper, D.A., Longstaffe, F.J., Wadleigh, M.A. and McNutt, R.H. (1995) Secondary K-feldspar
728 at the Precambrian-Paleozoic unconformity, southwestern Ontario. *Canadian Journal of Earth*
729 *Sciences*, 32, 1432-1450.
730 Hatcher, R.D. Jr. (2002) Alleghanian (Appalachian) orogeny, a product of zipper tectonics:
731 Rotational transpressive continent-continent collision and closing of ancient oceans along
732 irregular margins. In: Martínez Catalán, J.R., Hatcher, R.D.Jr., Arenas, R., and Díaz García,
733 F. (eds.), Variscan-Appalachian dynamics: The building of the late Paleozoic basement.
734 *Geological Society of America Special Paper,* 364, Boulder, Colorado, 199–208.

735 Hatcher, R.D. Jr. (2005) Regional geology of North America – Southern and Central
736 Appalachians. *Encyclopedia of Geology*, Elsevier, London, 72-81.
737 Hatcher, R.D. Jr., Thomas, W.A., Geiser, P.A., Snoke, A.W., Mosher, S. and Wiltschko, D.V.
738 (1989) Alleghanian Orogen. In: Hatcher, R.D., Jr., Thomas, W.A., and Viele, G.W. (eds.),
739 The Appalachian-Ouachita orogen in the United States. *Geology of North America, Vol. F-2,*
740 Boulder, Colorado, Geological Society of America, 233–318.
741 Hay, R.L., Lee, M. Kolata, D.R., Matthews, J.C. and Morton, J.P. (1988) Episodic potassic
742 diagenesis of Ordovician tuffs in the Mississippi Valley area. *Geology*, 16, 743-747.
743 Hearn, P.P. Jr and Sutter, J.F. (1985) Authigenic potassium feldspar in Cambrian carbonates:
744 evidence of Alleghanian brine migration. *Science*, 228, 1529-1531.
745 Hearn, P.P.Jr., Sutter, J.F. and Belkin, H.E. (1987) Evidence for Late-Paleozoic brine migration
746 in Cambrian carbonate rocks of the central and southern Appalachians: Implications for
747 Mississippi Valley-type sulfide mineralization. *Geochimica et Cosmochimica Acta*, 51, 1323-
748 1334.
749 Honty, M., Uhlík, P., Sucha, V., Caplovicová, M., Francù, J., Clauer, N. and Biron, A. (2004)
750 Smectite-to-illite alteration in salt-bearing bentonites (the East Slovak Basin). *Clays and Clay*
751 *Minerals*, 52, 533-551.
752 Horton, J.W., Jr., Drake, A.A. and Rankin, D.W. (1989) Tectonostratigraphic terranes and their
753 Paleozoic boundaries in the Central and Southern Appalachians. In: Dallmeyer, R.D., (ed.),
754 Terranes in the circum-Atlantic Paleozoic orogens. *Geological Society of America Special*
755 *Paper*, 230, 213–245.
756 Huff, W.D., Bergstrom, S.M. and Kolata, D.R. (1986) Gigantic Ordovician ash fall in North
757 America and Europe: biological, tectonomagmatic, and event-stratigraphic significance.
758 *Geology*, 20, 875-878.
759 Huff, W.D. and Kolata, D.R. (1990) Correlation of the Ordovician Deicke and Millbrig K-
760 bentonites between the Mississippi Valley and the southern Appalachians. *American*
761 *Association of Petroleum Geologists Bulletin*, 74, 1736-1747.
762 Jackson, M.L. (1975) Soil chemical analysis – advanced course. Madison, Wisconsin, 386p.
763 Kolata, D.R., Huff, W.D. and Bergström, S.M. (1996) Ordovician K-bentonites of eastern North
764 America. *Geological Society of America, Special Paper*, 313, 1-84.
765 Leslie, S.A., Bergström, S.M. and Huff, W.D. (2008) Ordovician K-bentonites discovered in

766 Oklahoma. *Oklahoma Geology Notes*, 68, 4-14.
767 Liu, J., Hay, R.L., Deino, A. and Kyser, T.K. (2003) Age and origin of authigenic K-feldspar in
768 uppermost Precambrian rocks in the North American Midcontinent. *Geological Society of*
769 *America Bulletin*, 115, 422-433.
770 Longstaffe, F.J. and Ayalon, A. (1990) Hydrogen-isotope geochemistry of diagenetic clay
771 minerals from Cretaceous sandstones, Alberta, Canada: Evidence for exchange. *Applied*
772 *Geochemistry*, 5, 657-668.
773 Macaulay, C.I., Fallick, A.E., Haszeldine, R.S. and , C.M. (2000) Methods of laser-based stable
774 isotope measurement applied to diagenetic cements and hydrocarbon reservoir quality. *Clay*
775 *Minerals*, 35, 317–326.
776 Marshall, B.D., Woodard, H.H. and DePaolo, D.J. (1986) K-Ca-Ar systematics of authigenic
777 sanidine from Waukau, Wisconsin, and the diffusivity of argon. *Geology*, 14, 936-938.
778 Moore, D. M. and Reynolds, R.C.Jr. (1997) X-Ray diffraction and the identification and analysis
779 of clay minerals. 2nd ed., *Oxford University Press*, New York, 378 p.
780 Nadeau, P.H., Wilson, M.J., McHardy, W.J. and Tait, J.M. (1984) Interstratified clays as
781 fundamental particles. *Science*, 225, 923-925.
782 Nadeau, P.H. and Bain, D.C. (1986) Composition of some smectites and diagenetic illitic clays
783 and implications for their origin. *Clays and Clay Minerals*, 34, 455-464.
784 Nier, A.O. (1950) A redetermination of the relative abundances of the isotopes of carbon,
785 nitrogen, oxygen, argon and potassium. *Physical Review*, 77, 789–793.
786 Odin, G.S. and 35 collaborators (1982) Interlaboratory standards for dating purposes. In: Odin
787 G.S. (ed.), Numerical Dating in Stratigraphy, *John Wiley & Sons*, Chichester, 123–148.
788 Oliver, J. (1986) Fluids expelled tectonically from orogenic belts: Their role in hydrocarbon
789 migration and other geologic phenomena. *Geology*, 14, 99-102.
790 Raymond, D.E., Osborne, W.E., Copeland, C.W. and Neathery, T.L. (1988) Alabama
791 stratigraphy. *Alabama Geological Survey Circular*, 140, 97p.
792 Roden, M.K., Elliott, W.C., Aronson, J.L. and Miller, D.S. (1993) Comparison of fission-track
793 ages of apatite and zircon to the K/Ar ages of illite-smectite (I/S) from Ordovician K-
794 bentonites, southern Appalachian basin. *Journal of Geology*, 101, 633-641.

795 Smith, L.B. Jr. (2006) Origin and Reservoir Characteristics of Upper Ordovician Trenton-Black
796 River Hydrothermal Dolomite Reservoirs in New York. *American Association of Petroleum*
797 *Geologists Bulletin*, 90, 1691-1718.
798 Środoń, J. (1981) X-ray identification of randomly interstratified illite-smectite in mixtures with
799 discrete illite. *Clay Minerals*, 16, 297-304.
800 Środoń, J., Elsass, F., McHardy, W.J. and Morgan, D.J. (1992) Chemistry of illite/smectite
801 inferred from TEM measurements of fundamental particles. *Clay Minerals*, 27, 137-158.
802 Środoń, J. and Clauer, N. (2001) Diagenetic history of Lower Palaeozoic sediments in Pomerania
803 (northern Poland) traced across the Teisseyre-Tornquist tectonic zone using mixed-layer illite-
804 smectite. *Clay Minerals*, 36, 15-27.
805 Środoń, J., Clauer, N., Banas, M. and Wojtowicz, A. (2006) K-Ar evidence for a Mesozoic
806 thermal event superimposed on burial diagenesis of the Upper Silesia Coal Basin. *Clay*
807 *Minerals*, 41, 669-690.
808 Stamatakos, J., Hirt, A.M. and Lowrie, W. (1996) The age and timing of folding in the central
809 Appalachians from paleomagnetic results. *Geological Society of America Bulletin*, 108, 815-
810 829.
811 Steiger, R.H. and Jäger, E. (1977) Subcommission on Geochronology: convention on the use of
812 decay constants in geochronology and cosmochronology. *Earth and Planetary Science Letters*,
813 36, 359–362.
814 Szabo, M.W., Osborne, W.E., Copeland, C.W.Jr. and Neathery, T.L. (1988) Geologic map of
815 Alabama. *Alabama Geological Survey, Special Map 220*, scale 1:250,000.
816 Toulkeridis, T., Clauer, N., Chaudhuri, S. and Goldstein, S.L. (1998) Multi-method (K-Ar, Rb-Sr,
817 Sm-Nd) dating of bentonite minerals from eastern United States. *Basin Research*, 10, 261-270.
818 Woodard, H.H. (1972) Syngenetic sanidine beds from Middle Ordovician Saint Peter Sandstone,
819 Wisconsin. *Journal of Geology*, 80, 323-332.
820 Ziegler, K. and Longstaffe, F.J. (2000a) Multiple episodes of clay alteration at the
821 Precambrian/Paleozoic unconformity, Appalachian basin: isotopic evidence for long-distance
822 and local fluid migrations. *Clays and Clay Minerals*, 48, 474-493.
823 Ziegler, K. and Longstaffe, F.J. (2000b) Clay mineral authigenesis along a mid-continental scale
824 fluid conduit in Palaeozoic sedimentary rocks from southern Ontario, Canada. *Clay Minerals*,
825 35, 239-260.

826
827
828
829
830

FIGURE AND TABLE CAPTION

832

833 **Figure 1:** Geographic location of the sampling sites. From north to south, sample 3B was
834 collected near Trenton, samples 1A, 1B, 2A, 2B, 2C and 4B come from near Dalton, sample 3A
835 was taken near Lafayette and sample 4A at Dirtseller Mountain.

836

837 **Figure 2:** XRD patterns of the air-dried (A) and ethylene-glycolated (B) size fractions of sample
838 4A.

839

840 **Figure 3:** XRD patterns of the polymer PVP-treated size fractions of sample 4A.

841

842 **Figure 4:** Measured vs. calculated XRD pattern of a size fraction from sample 4A.

843

844 **Figure 5:** Measured vs. StackMan-calculated XRD pattern of the glycolated 0.1-0.2 μm size
845 fraction from the sample 4A. The pattern was calculated from the crystallite size distribution and
846 the 2:1 layer parameters found in Eberl et al. (2011), using a variable Lp factor with an
847 orientation function (sigma*) of 2.3.

848

849 **Figure 6:** Alpha-beta^2 diagram for the different nanometric size fractions of the studied samples.
850 Most data points (grey circles) plot near the nucleation + growth curve. Only three fractions
851 plot away on the surface-controlled curve. The black triangles represent hydrothermal
852 bentonites from another study (Eberl et al., 1998b) and the black rectangles represent
853 diagenetic illite/smectite mixed-layers from East Slovak Basin (Sucha, unpublished data).

854

Figure 7: Mean thickness in nm, by area (the black diamonds) and volume (the grey squares) weight, relative to the K-Ar ages of the different nanometric size fractions.

Figure 8: $^{40}Ar/^{36}Ar$ vs. $^{40}K/^{36}Ar$ isochron diagram of the different studied nanometric size fractions. The grey symbols define the upper isochron, the open ones the lower isochron and the black ones fall off the two lines, either in between or above the upper line.

Figure 9: $\delta^{18}O$ vs. δD (A) and $\delta^{18}O$ vs. K-Ar (B) plots for the different studied nanometric size fractions.

Table 1: XRD results on the studied size fractions.

Table 2: $\delta^{18}O$ and δD values for the studied size fractions.

Table 3: K-Ar data of the studied size fractions.

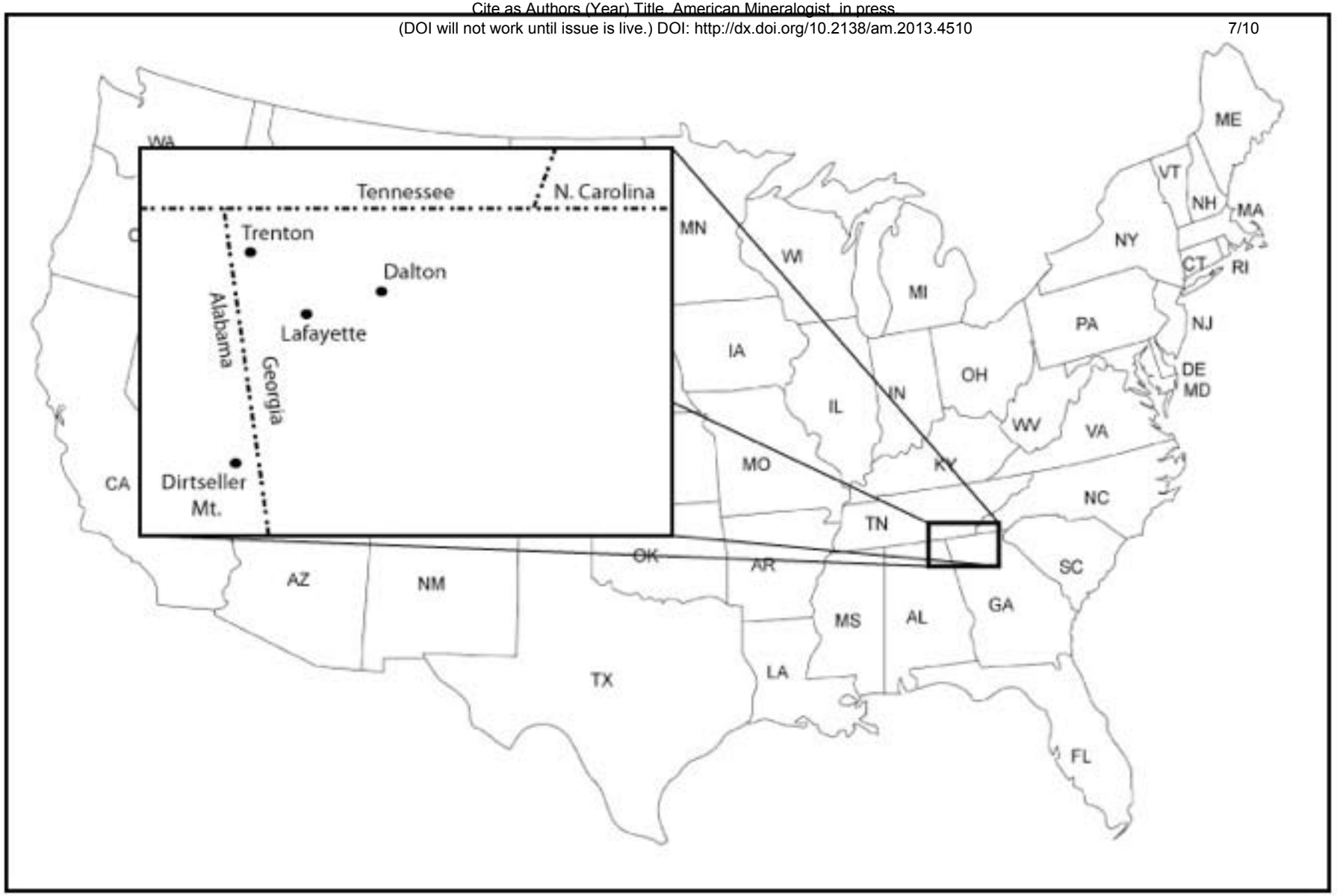
Tennessee
N. Carolina
Trenton
Dalton
Lafayette
Alabama
Georgia
Dirtseller
Mt.
WA
CA
AZ
NM
TX
OK
AR
LA
MS
AL
GA
FL
SC
NC
TN
KY
WV
VA
OH
IN
IL
MO
IA
MN
WI
MI
NY
PA
ME
VT
NH
MA
CT
RI
NJ
DE
MD

Figure 1

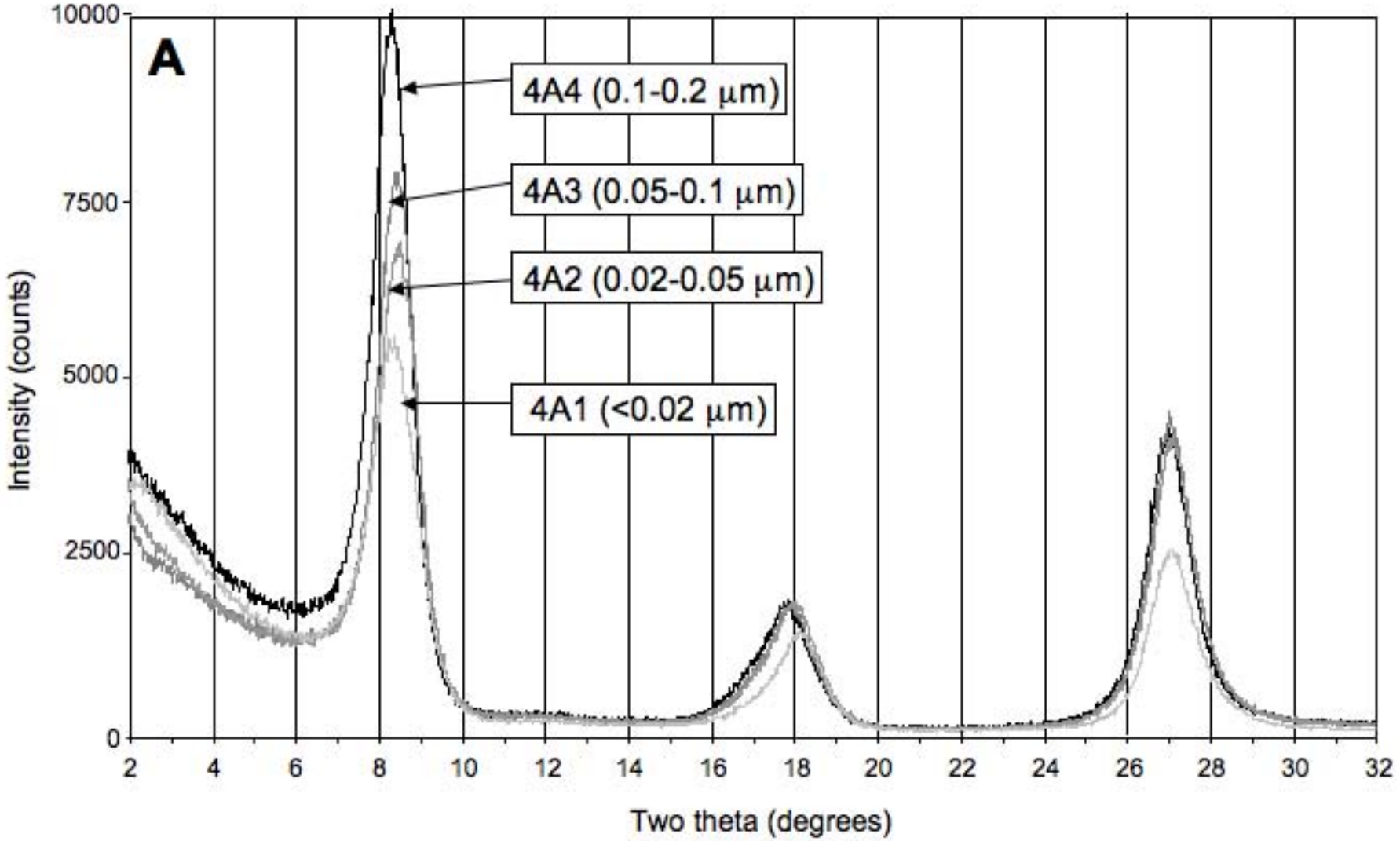
A
4A4 (0.1-0.2 μm)
4A3 (0.05-0.1 μm)
4A2 (0.02-0.05 μm)
4A1 (<0.02 μm)
Intensity (counts)
10000
7500
5000
2500
0
2
4
6
8
10
12
14
16
18
20
22
24
26
28
30
32
Two theta (degrees)

Figure 2A

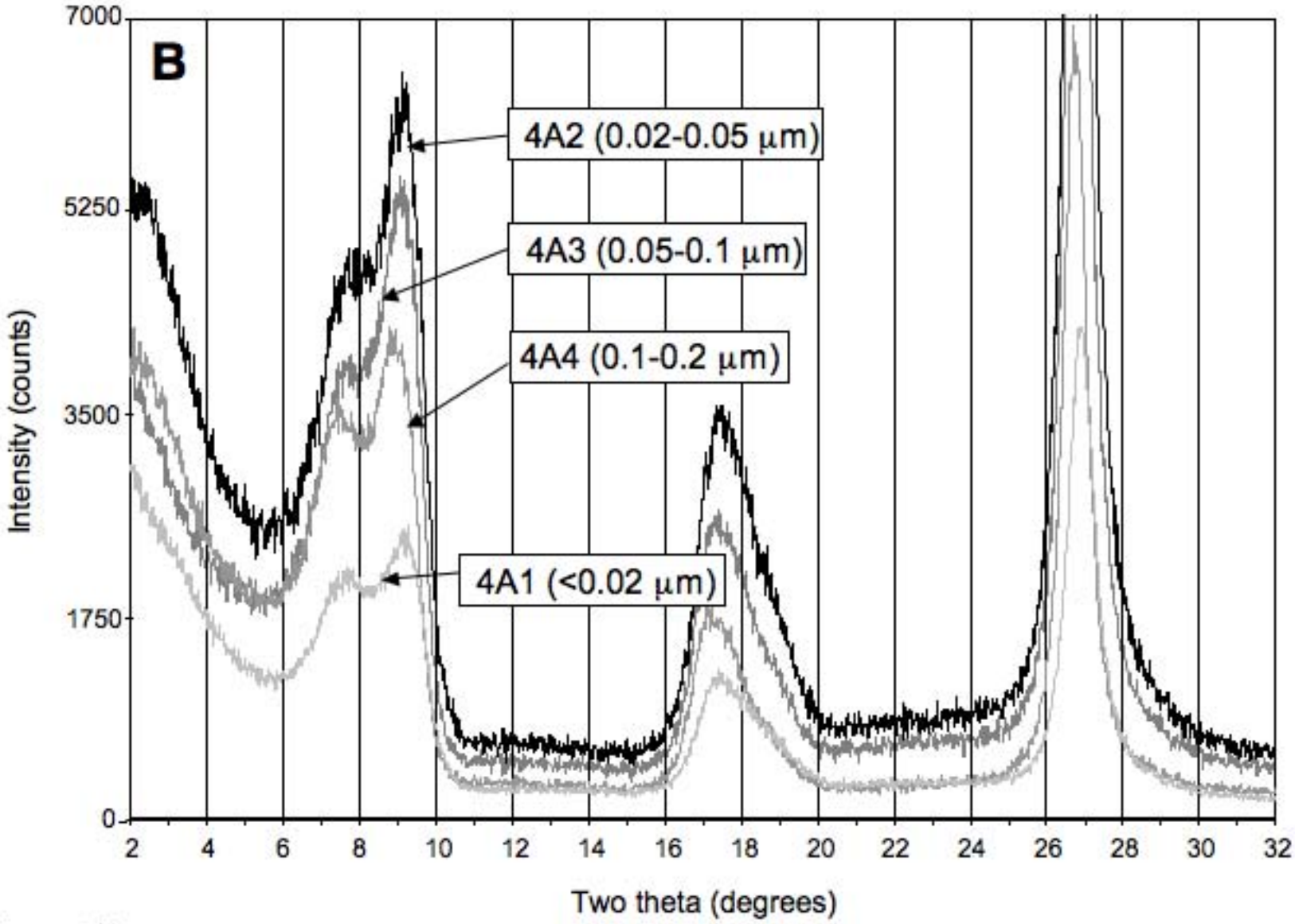

Figure 2B

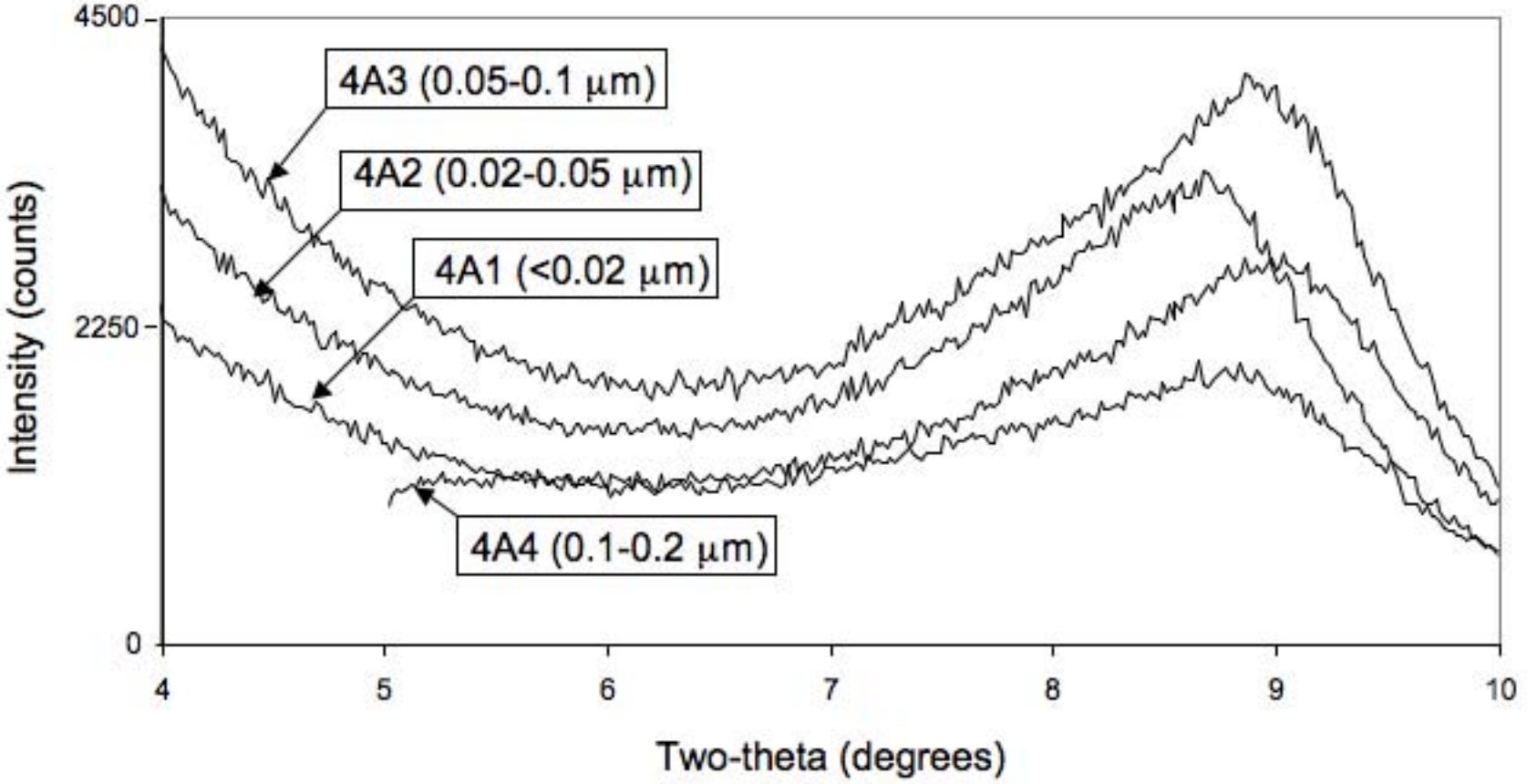
4500
2250
0
Intensity (counts)
4A3 (0.05-0.1 μm)
4A2 (0.02-0.05 μm)
4A1 (<0.02 μm)
4A4 (0.1-0.2 μm)
4
5
6
7
8
9
10
Two-theta (degrees)

Figure 3

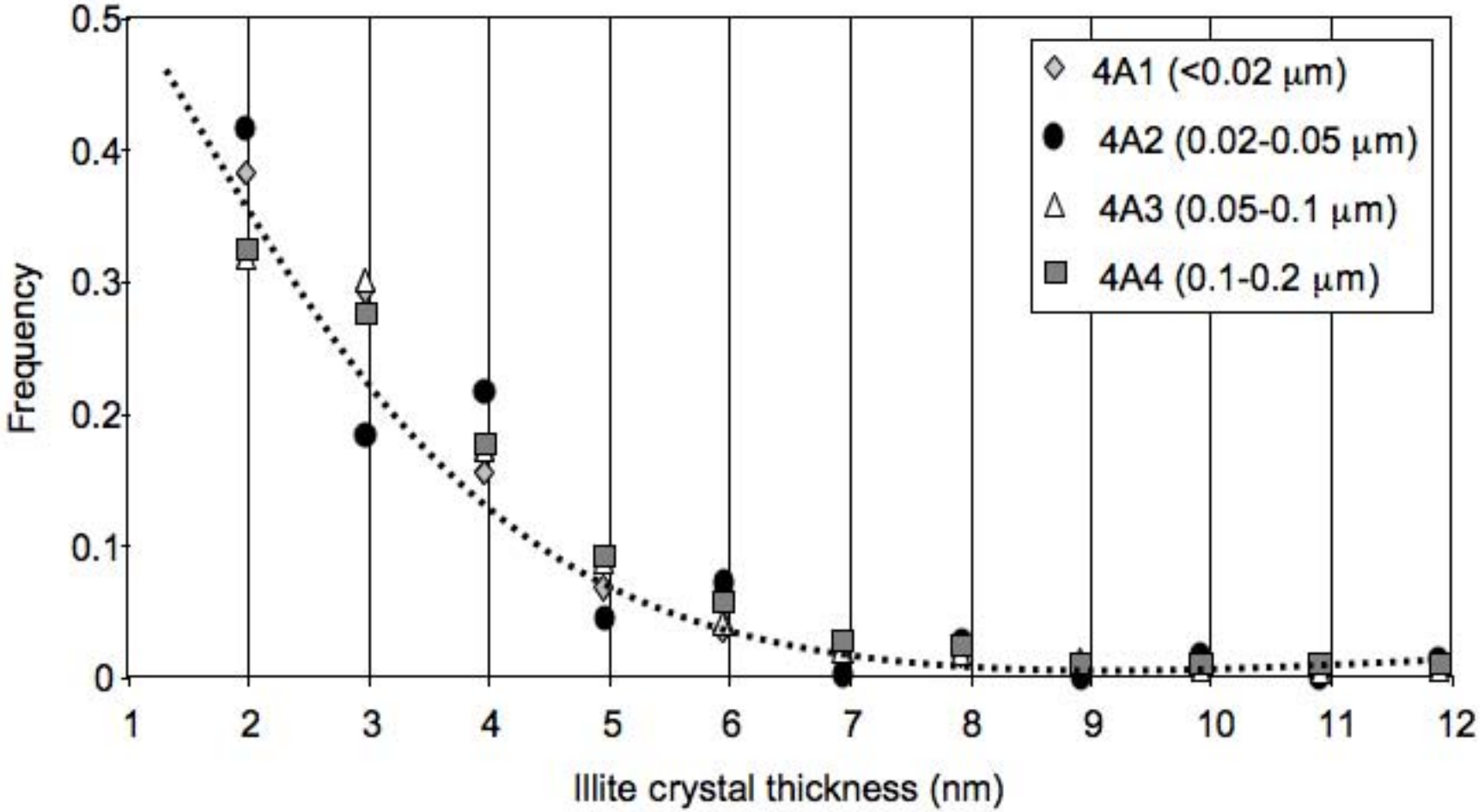
0.5
0.4
0.3
0.2
0.1
0
Frequency
1
2
3
4
5
6
7
8
9
10
11
12
Illite crystal thickness (nm)
4A1 (<0.02 μm)
4A2 (0.02-0.05 μm)
4A3 (0.05-0.1 μm)
4A4 (0.1-0.2 μm)

Figure 4

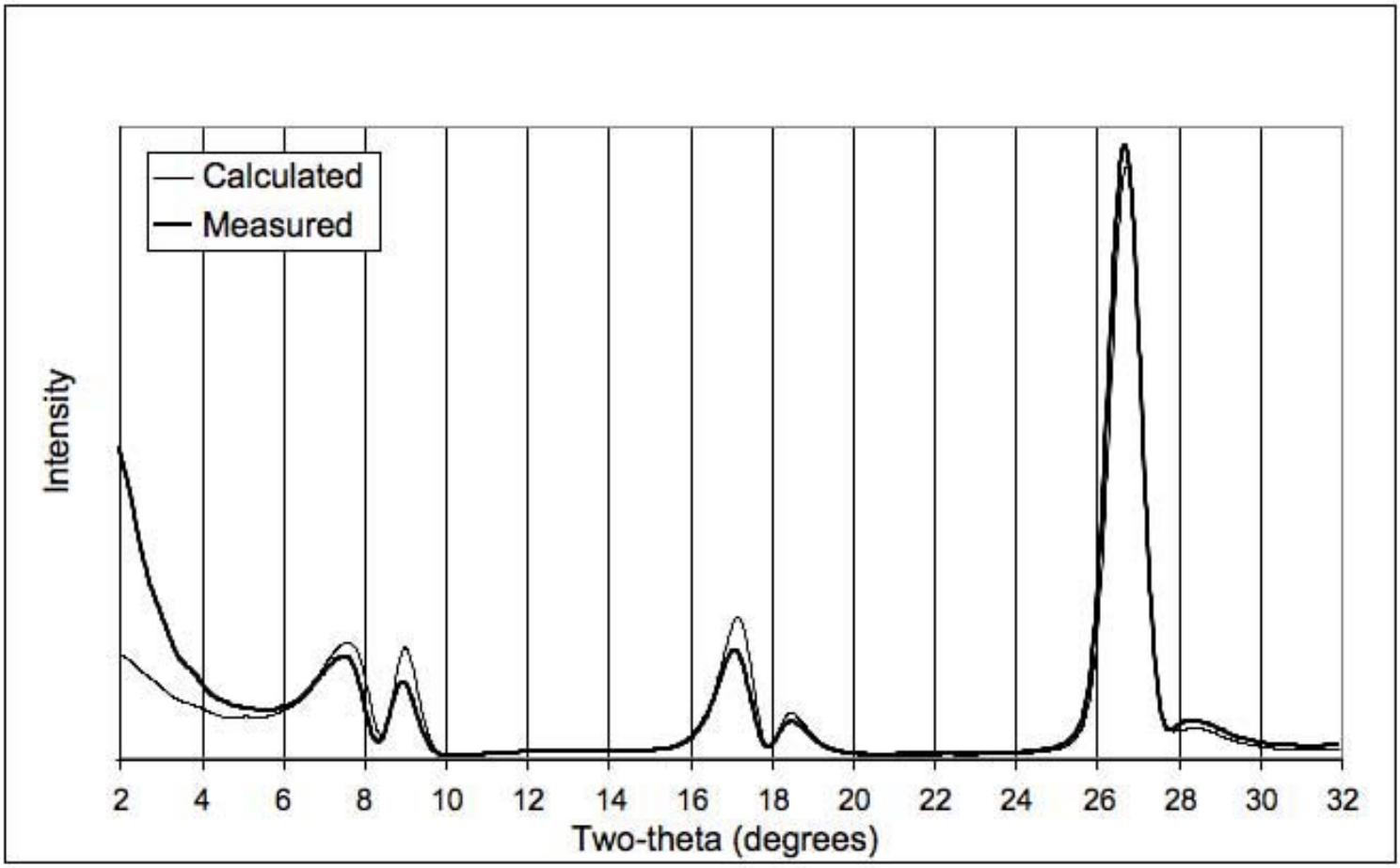
Calculated
Measured
Intensity
2
4
6
8
10
12
14
16
18
20
22
24
26
28
30
32
Two-theta (degrees)

Figure 5

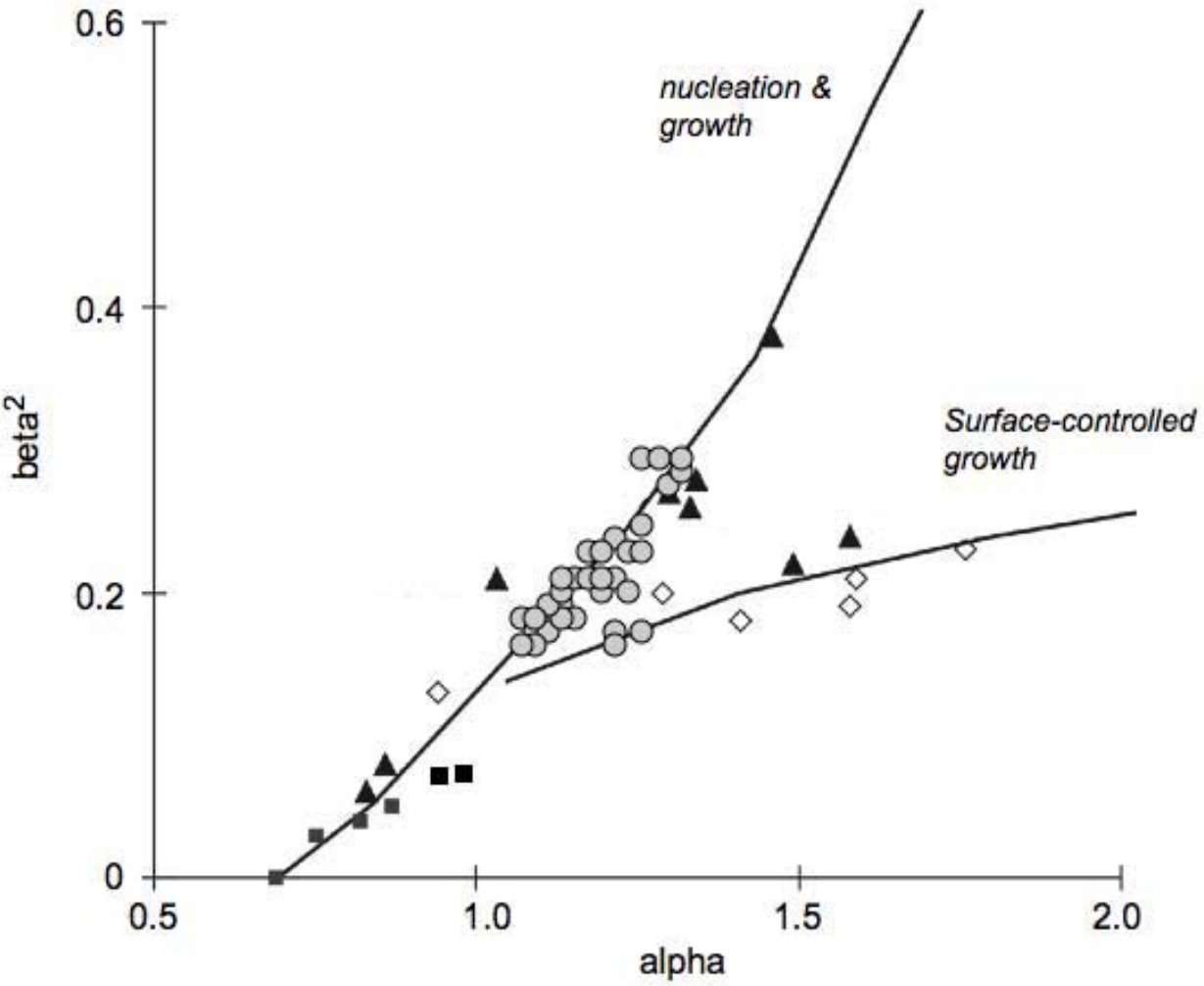
0.6
0.4
0.2
0
beta2
0.5
1.0
1.5
2.0
alpha
nucleation &
growth
Surface-controlled
growth

Figure 6

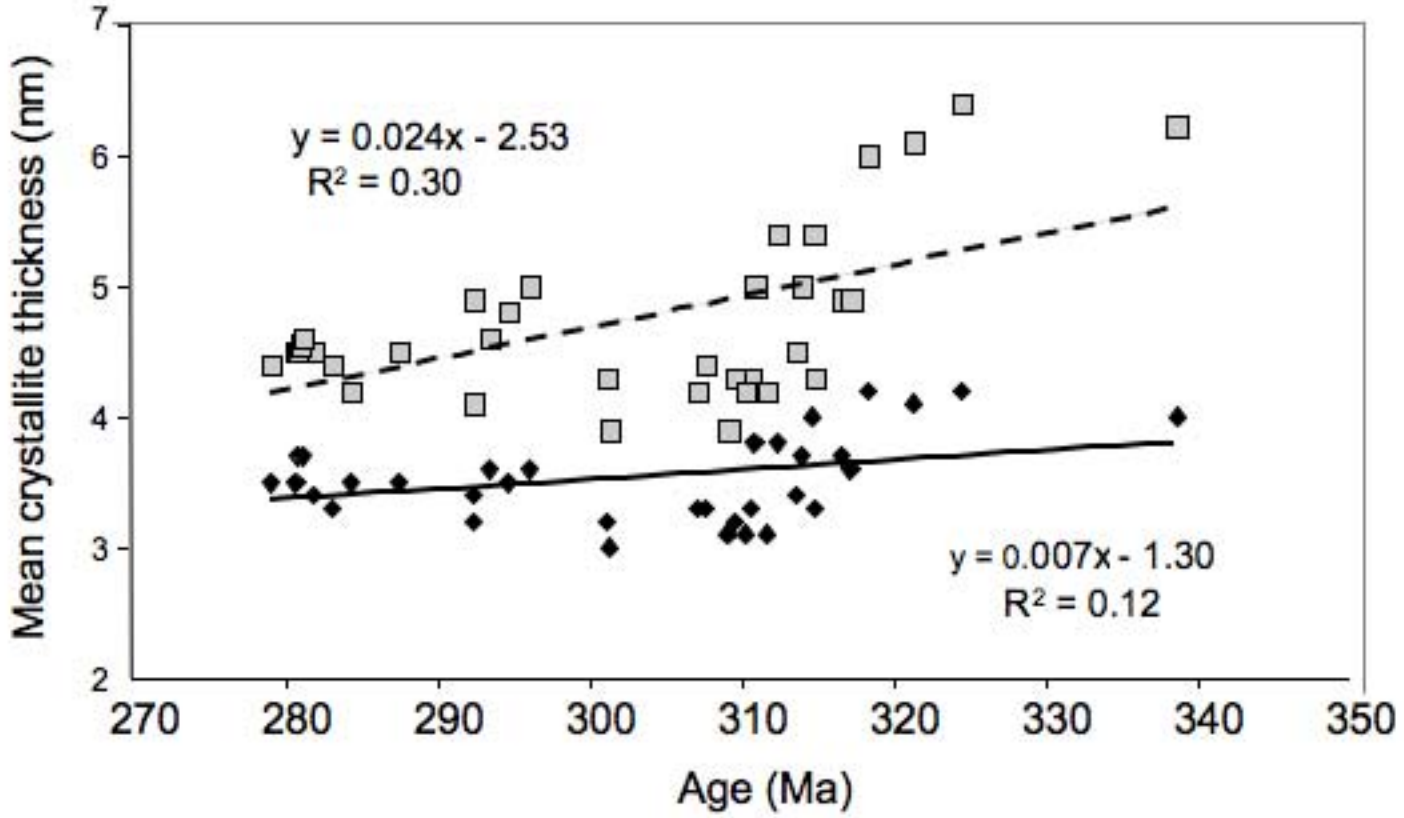
Mean crystallite thickness (nm)
7
6
5
4
3
2
y = 0.024x - 2.53
R² = 0.30
y = 0.007x - 1.30
R² = 0.12
270
280
290
300
310
320
330
340
350
Age (Ma)

Figure 7

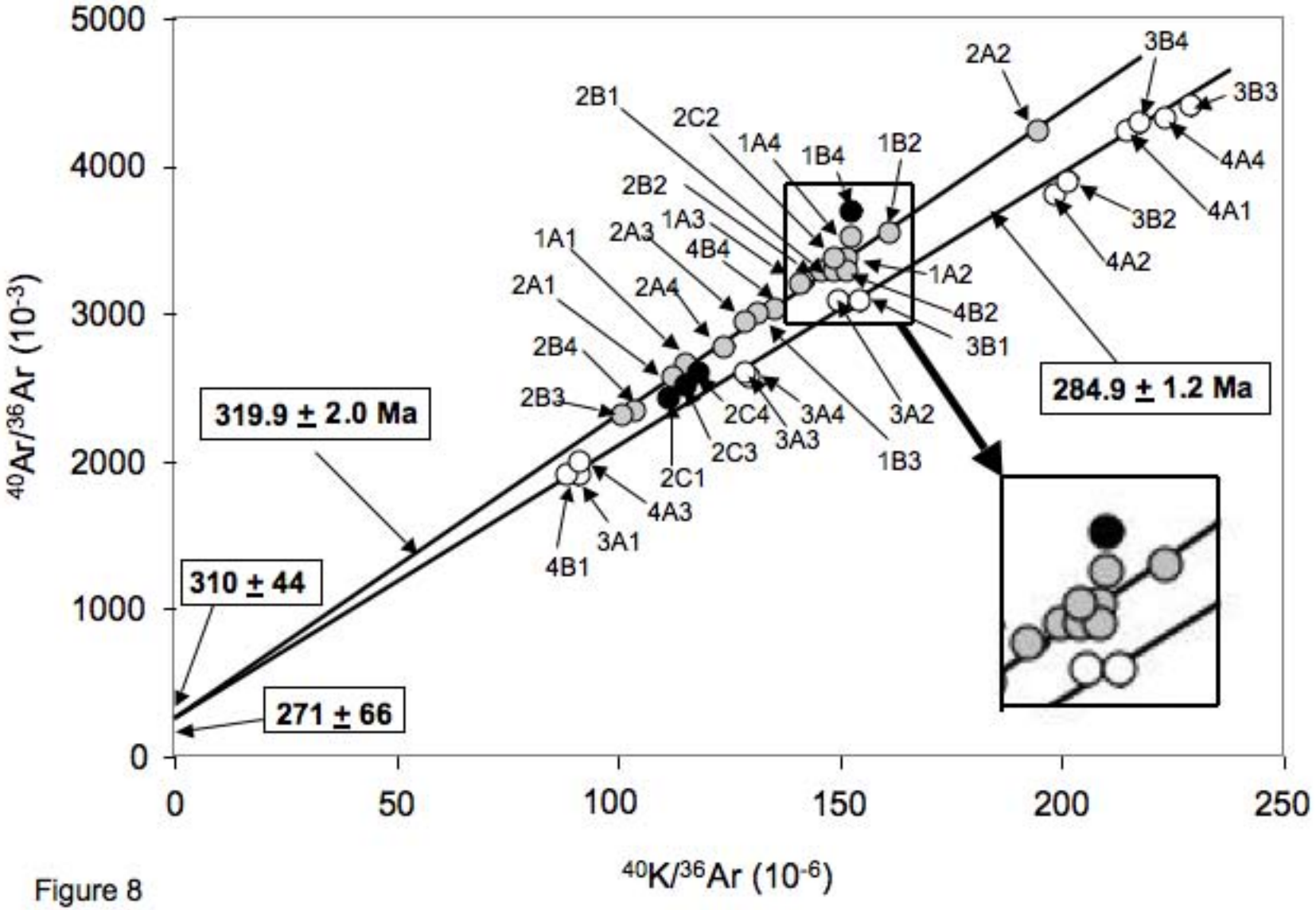
5000
4000
3000
2000
1000
0
0
50
100
150
200
250
$^{40}Ar/^{36}Ar$ (10^{-3})
$^{40}K/^{36}Ar$ (10^{-6})
319.9 ± 2.0 Ma
310 ± 44
271 ± 66
284.9 ± 1.2 Ma
2B1
2C2
1A4
1B4
1B2
2A2
3B4
3B3
4A4
2B2
1A3
2A3
4B4
1A1
2A1
2A4
1A2
4B2
3B1
3B2
4A1
4A2
2B4
2B3
2C4
3A4
3A2
3A3
2C3
1B3
2C1
4A3
3A1
4B1

Figure 8

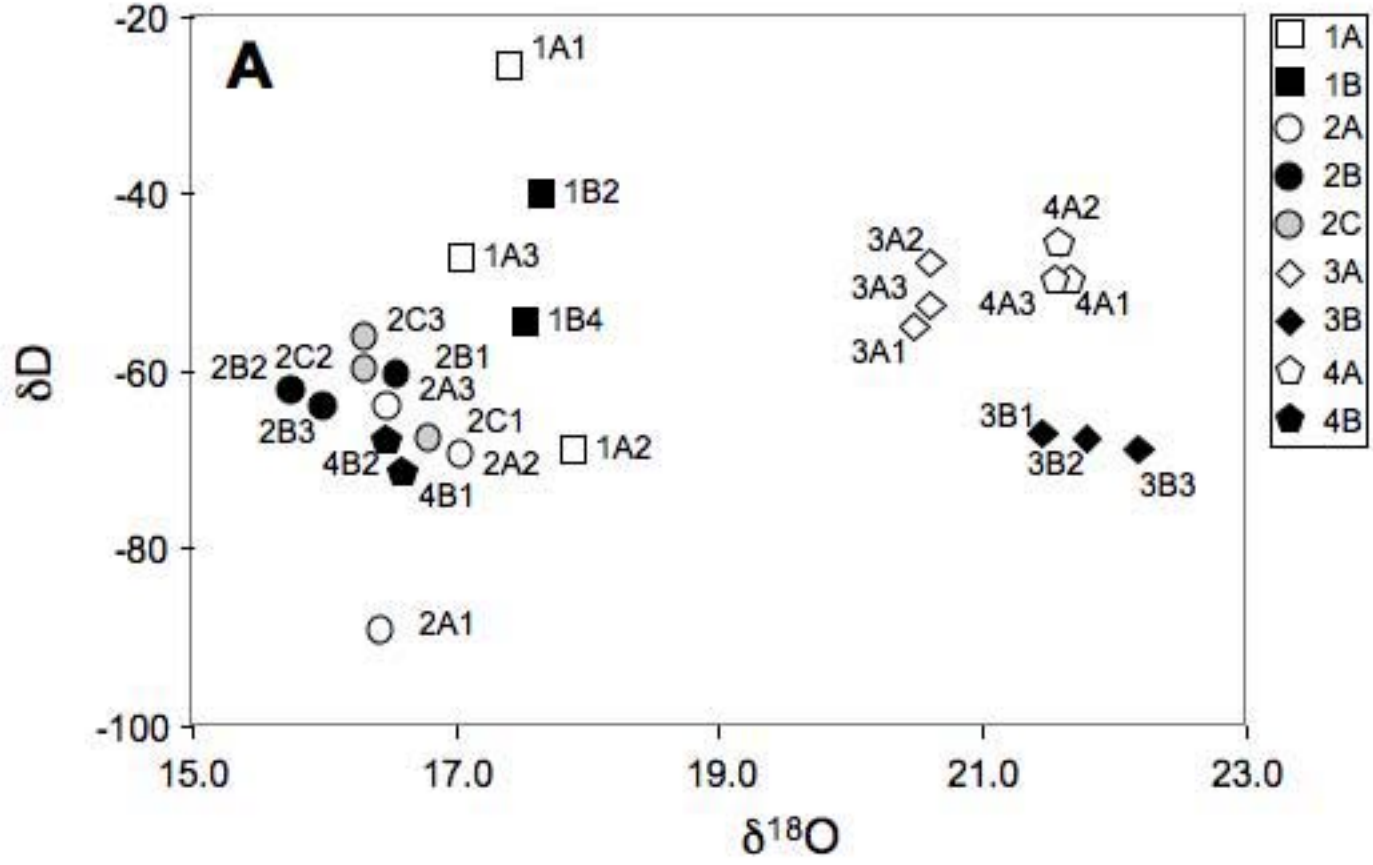
A
δD
δ18O
-20
-40
-60
-80
-100
15.0
17.0
19.0
21.0
23.0
1A1
1B2
1A3
1B4
2C3
2B2
2C2
2B1
2A3
2B3
2C1
2A2
1A2
4B2
4B1
2A1
3A2
3A3
3A1
4A2
4A3
4A1
3B1
3B2
3B3
1A
1B
2A
2B
2C
3A
3B
4A
4B

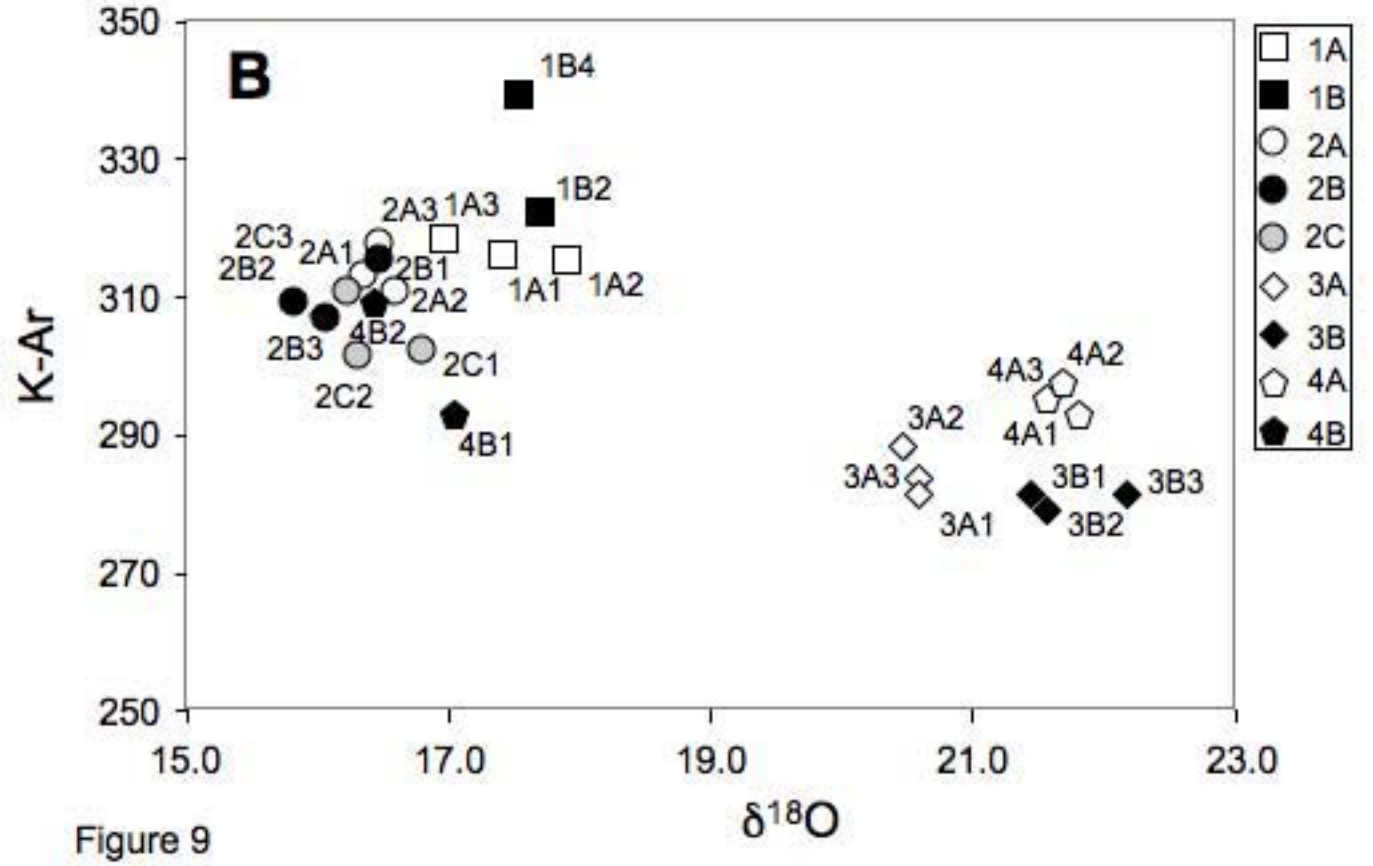
B
K-Ar
δ18O
350
330
310
290
270
250
15.0
17.0
19.0
21.0
23.0
1B4
1B2
2A3
1A3
2C3
2A1
2B2
2B1
1A1
1A2
2A2
2B3
4B2
2C1
2C2
4B1
4A3
4A2
4A1
3A2
3A3
3A1
3B1
3B2
3B3
1A
1B
2A
2B
2C
3A
3B
4A
4B

Figure 9

Table 1

Samples	Size	smectite layers	kaolinite	Mean crystallite thickness (nm)	
	(m)	(%)		Area weighted	Volume weighted
1A = base of Deicke Formation (T3 bentonite unit) at Dalton, Georgia					
1A1	< 0.02	11	N	3.7	4.9
1A2	0.02-0.05	11	N	4.0	5.4
1A3	0.05-0.1	12	Y	4.2	6.0
1A4	0.1-0.2	10	Y	4.2	6.4
1B (= top of the unit)					
1B2	0.02-0.05	8	Y	3.7	5.0
1B3	0.05-0.1	7	Y	4.1	6.1
1B4	0.1-0.2	6	Y	4.0	6.3
2A = base of Deicke Formation (T3 bentonite unit) at Dalton, Georgia					
2A1	< 0.02	19	N	3.8	5.4
2A2	0.02-0.05	18	N	3.8	5.0
2A3	0.05-0.1	19	N	3.6	4.9
2A4	0.1-0.2	22	N	3.4	4.5
2B = middle of the unit					
2B1	< 0.02	17	N	3.3	4.3
2B2	0.02-0.05	20	Y	3.3	4.3
2B3	0.05-0.1	20	Y	3.3	4.2
2B4	0.1-0.2	20	Y	3.1	3.9
2C = top of the unit					
2C1	< 0.02	13	N	3.0	3.9
2C2	0.02-0.05	13	Y	3.2	4.3
2C3	0.05-0.1	18	Y	3.1	4.2
2C4	0.1-0.2	18	Y	3.3	4.4
4B = Millbrig Formation at Dalton, Georgia					
4B1	< 0.02	18	N	3.2	4.1
4B2	0.02-0.05	18	N	3.2	4.3

4B4	0.1-0.2	21	N	3.1	4.2
3A = Deicke Formation of Lafayette, Georgia					
3A1	< 0.02	22	N	3.5	4.5
3A2	0.02-0.05	22	N	3.5	4.5
3A3	0.05-0.1	22	N	3.4	4.5
3A4	0.1-0.2	23	N	3.3	4.4
3B = South of Trenton, Georgia					
3B1	< 0.02	15	N	3.5	4.4
3B2	0.02-0.05	14	N	3.7	4.5
3B3	0.05-0.1	16	N	3.7	4.6
3B4	0.1-0.2	17	N	3.5	4.2
4A = Millbrig Formation at Dirtseller, Alabama					
4A1	< 0.02	13	N	3.4	4.9
4A2	0.02-0.05	12	N	3.5	4.8
4A3	0.05-0.1	12	N	3.6	5.0
4A4	0.1-0.2	13	N	3.6	4.6

N stands for no and Y for yes

Table 2

Samples	Size (mm)	Yields (mmol/mg)	$d^{18}O$ (V-SMOW)	dD (V-SMOW)
1A = base of T3 bentonite unit at Dalton, Georgia				
1A1	< 0.02	2.2	17.4	-26
1A2	0.02-0.05	3.1	17.9	-70
1A3	0.05-0.1	3.1	17.0	-47
1B = top of the unit				
1B2	0.05-0.1	4.1	17.7	-41
1B4	0.1-0.2	4.2	17.5	-54
2A = base of T3 bentonite unit at Dalton, Georgia				
2A1	< 0.02	3.4	16.4	-90
2A2	0.02-0.05	3.2	16.6	-71
2A3	0.05-0.1	2.7	16.5	-64
2B = middle of the unit				
2B1	< 0.02	3.1	16.5	-61
2B2	0.02-0.05	2.9	15.8	-62
2B3	0.05-0.1	2.8	16.0	-64
2C = top of the unit				
2C1	< 0.02	3.3	16.8	-68
2C2	0.02-0.05	3.1	16.3	-60
2C3	0.05-0.1	3.0	16.3	-57
3A = Deicke Formation of Lafayette, Georgia				
3A2	0.02-0.05	3.1	20.5	-55
3A3	0.05-0.1	3.0	20.6	-48
3A4	0.1-0.2	2.7	20.6	-53

3B = South of Trenton, Georgia				
3B1	< 0.02	3.3	21.6	-50
3B2	0.02-0.05	2.7	22.2	-69
3B3	0.05-0.1	2.7	21.5	-67
4A = Millbrig Formation at Dirtseller, Alabama				
4A1	< 0.02	3.3	21.8	-68
4A2	0.02-0.05	2.9	21.6	-47
4A3	0.05-0.1	2.9	21.7	-50
4B = Millbrig Formation at Dalton, Georgia				
4B1	< 0.02	3.3	17.0	-70
duplicate			16.8	
4B2	0.02-0.05	2.7	16.5	-68
duplicate			16.2	

Table 3

Samples	Size (m)	K_2O (%)	Ar* (%)	$^{40}Ar^*$ (10^{-6} cm^3/g)	$^{40}Ar/^{36}Ar$ (10^{-3})	$^{40}K/^{36}Ar$ (10^{-6})	Age (Ma ± 2)	Average
1A = base of T3 bentonite unit at Dalton, Georgia								
1A1	< 0.02	4.69	88.85	52.31	2650	116	316.6 (7.7)	318
1A2	0.02-0.05	4.90	91.19	54.30	3353	151	314.7 (7.5)	+
1A3	0.05-0.1	5.51	90.78	61.82	3204	142	318.3 (7.5)	-
1A4	0.1-0.2	5.43	91.53	62.20	3490	153	324.4 (7.6)	5
1B = top of the unit								
1B2	0.02-0.05	4.79	91.69	52.94	3558	161	314.0 (7.4)	317
1B3	0.05-0.1	4.68	90.21	53.06	3017	132	321.4 (7.7)	±
1B4	0.1-0.2	4.35	91.95	52.21	3672	154	338.6 (8.1)	3
2A = base of T3 bentonite unit at Dalton, Georgia								
2A1	< 0.02	6.05	88.47	66.49	2562	113	312.4 (7.4)	312
2A2	0.02-0.05	6.13	92.96	67.03	4196	195	310.9 (7.1)	+
2A3	0.05-0.1	6.06	90.06	67.73	2974	131	317.2 (7.4)	-
2A4	0.1-0.2	6.16	89.39	67.98	2785	124	313.6 (7.4)	3
2B = middle of the unit								
2B1	< 0.02	5.64	90.96	62.52	3267	147	314.8 (7.4)	310
2B2	0.02-0.05	5.96	90.87	64.97	3237	148	310.0 (7.2)	
	0.02-0.05 du	5.92	89.85	64.65	2911	131	310.6 (7.3)	+
2B3	0.05-0.1	6.11	87.05	65.92	2282	91	307.1 (7.4)	-
2B4	0.1-0.2	6.12	87.45	66.49	2354	104	309.1 (7.4)	3
2C = top of the unit								
2C1	< 0.02	5.15	87.90	54.42	2443	113	301.3 (7.3)	305
2C2	0.02-0.05	5.56	90.72	58.74	3184	149	301.2 (7.1)	+
2C3	0.05-0.1	5.59	88.32	61.30	2531	116	311.7 (7.5)	-
2C4	0.1-0.2	5.66	88.52	61.18	2574	117	307.7 (7.4)	5
3A = Deicke Formation of Lafayette, Georgia								
3A1	< 0.02	5.89	84.49	57.64	1905	91	280.7 (7.0)	283

3A2	0.02-0.05	6.01	90.28	60.38	3040	150	287.5 (6.7)	+
3A3	0.05-0.1	6.31	88.63	62.02	2599	129	281.8 (6.7)	-
3A4	0.1-0.2	6.30	88.66	62.20	2606	128	283.0 (6.7)	3
3B = South of Trenton, Georgia								
3B1	< 0.02	6.33	90.28	61.58	3040	155	279.1 (6.5)	281
3B2	0.02-0.05	6.56	92.45	64.23	3912	202	280.8 (6.4)	+
3B3	0.05-0.1	6.63	93.30	64.98	4409	229	281.1 (6.3)	-
3B4	0.1-0.2	6.56	93.08	65.09	4270	218	284.3 (6.4)	2
4A = Millbrig Formation at Dirtseller Mountain, Alabama								
4A1	< 0.02	5.95	93.97	60.85	4262	215	292.4 (6.1)	293
4A2	0.02-0.05	6.17	93.07	60.20	3770	199	294.6 (6.7)	+
4A3	0.05-0.1	6.31	91.90	65.40	1960	91	296.0 (6.3)	-
4A4	0.1-0.2	6.28	93.15	64.49	4315	223	293.4 (6.7)	2
4B (= Millbrig Formation at Dalton, Georgia)								
4B1	< 0.02	5.09	85.01	52.07	1971	90	292.4 (7.6)	304
4B2	0.02-0.05	5.41	90.98	58.89	3275	150	309.6 (7.3)	$\pm$
4B4	0.1-0.2	5.66	90.14	61.73	2997	136	310.2 (7.3)	6